Skew-symmetric Nitsche's formulation in isogeometric analysis: Dirichlet and symmetry conditions, patch coupling and frictionless contact

Qingyuan Hu, Franz Chouly, Ping Hu, Gengdong Cheng, Stéphane Pierre Alain Bordas

Skew-symmetric Nitsche's formulation in isogeometric analysis: Dirichlet and symmetry conditions, patch coupling and frictionless contact

Qingyuan Hu[a,b], Franz Chouly[c], Ping Hu[a], Gengdong Cheng[a], Stéphane P.A. Bordas[b,c,d,e,*]

[a] *State Key Laboratory of Structural Analysis for Industrial Equipment, Dalian University of Technology, P.R. China*
[b] *Institute of Computational Engineering, Faculty of Sciences Technology and Communication, University of Luxembourg, Luxembourg*
[c] *Laboratoire de Mathématiques de Besançon - UMR CNRS 6623, Université Bourgogne Franche-Comté, 16 route de Gray, 25030 Besançon cedex, France*
[d] *Institute of Mechanics and Advanced Materials, School of Engineering, Cardiff University, UK*
[e] *Intelligent Systems for Medicine Laboratory, University of Western Australia, Perth, Australia*

Abstract

A simple skew-symmetric Nitsche's formulation is introduced into the framework of isogeometric analysis (IGA) to deal with various problems in small strain elasticity: essential boundary conditions, symmetry conditions for Kirchhoff plates, patch coupling in statics and in modal analysis as well as Signorini contact conditions. For linear boundary or interface conditions, the skew-symmetric formulation is parameter-free. For contact conditions, it remains stable and accurate for a wide range of the stabilization parameter. Several numerical tests are performed to illustrate its accuracy, stability and convergence performance. We investigate particularly the effects introduced by Nitsche's coupling, including the convergence performance and condition numbers in statics as well as the extra "outlier" frequencies and corresponding eigenmodes in structural dynamics. We present the Hertz test, the block test, and a 3D self-contact example showing that the skew-symmetric Nitsche's formulation is a suitable approach to simulate contact problems in IGA.

Keywords: Isogeometric, Nitsche, parameter-free, contact, patch coupling, boundary conditions.

1. Introduction

The key concept in isogeometric analysis (IGA) [50] consists in using non-uniform rational B-splines (NURBS) as basis functions to approximate both the geometry and the unknown physical fields. The mathematical foundations of IGA are developed in [11], and a recent overview is given in [63]. Contrary to classical Lagrange basis functions usually adopted in the finite element method (FEM), NURBS in IGA

*Corresponding author
Email addresses: huqingyuan@mail.dlut.edu.cn (Qingyuan Hu), franz.chouly@univ-fcomte.fr (Franz Chouly), pinghu@dlut.edu.cn (Ping Hu), chenggd@dlut.edu.cn (Gengdong Cheng), stephane.bordas@alum.northwestern.edu (Stéphane P.A. Bordas)

have the ability to exactly describe geometries: thus, no geometrical approximation error is introduced. Moreover NURBS are widely adopted in commercial computer-aided design (CAD) packages, and this CAD data can directly be used to construct approximations. In boundary element method (BEM), this translates into the ability to solve directly from the field variables at the control points defining the geometry [78, 77, 74, 59, 10, 60, 58, 68]. In FEM, a 3D parameterization of the volume is still necessary [87, 88], except when solving shell-like problems [53, 13, 14, 38, 49]. The present paper focuses on two following issues. One first issue in IGA is related to boundary conditions, especially essential boundary conditions. Indeed, since NURBS are non-interpolatory, enforcing boundary conditions and constraints cannot be done as simply as in Lagrange FEM: they require tackling difficulties which are similar to those encountered in meshless methods [66] and implicit/immersed boundary methods [37, 46]. One second issue in IGA comes from interface conditions and patch coupling: for complex geometries, patch-wise CAD modeling is necessary, and transmission conditions need to be satisfied. The same also arises when gluing heterogeneous materials.

Various methods already exist to treat boundary or interface conditions weakly, that have been firstly designed for instance in the FEM context. They are applicable, or have already been applied, for IGA. The most widespread ones are the penalty method, mixed/mortar methods and Nitsche's method. The penalty method [7, 54] is simple but not consistent. Therefore the value of the penalty parameter has to be chosen with great care to achieve the best balance between accuracy and stability. As a matter of fact, if the penalty parameter is chosen too small the boundary or interface conditions are imposed inaccurately, whereas if it is chosen much larger than needed the penalized problem becomes ill-conditioned. Mixed methods for boundary conditions [6] introduce a Lagrange multiplier, which is an additional variable that represents the boundary stress, and that allows to take into account weakly the essential boundary conditions in a consistent way. This leads to a weak problem that has a saddle-point structure. For patch-coupling, the original mortar method [15, 16] has been reformulated later as a mixed/dual Lagrange multiplier method (see, e.g., [12, 84] for FEM and [18] for IGA). Mortar methods, when carefully designed, are consistent, stable and optimally accurate (see, e.g., [84] in the FEM context or [18] in the IGA context). Moreover the newly introduced Lagrange multipliers have a clear meaning: they are the stresses needed to enforce the continuity of the displacements. Mortar techniques have been applied as well with success to contact problems [81, 82, 33, 55, 75, 3]. However extra degrees of freedoms (DoFs) are introduced and an inf-sup condition must be fulfilled in order to ensure stability and optimal convergence, for which care is needed to build the dual space of Lagrange multipliers.

Nitsche's method was originally proposed by J. Nitsche [67, 79] to impose weakly essential boundary

conditions and more recently has regained popularity to deal with interface conditions with non-conforming discretizations (see, e.g., [9, 44, 2]). Nowadays Nitsche's method has also found a number of natural applications in IGA [40, 64, 4, 71, 42, 36]. Nitsche's formulation makes use of an appropriate *conjugate pair* such as displacement–force or rotation–moment, in such a way that the method remains both primal (no extra DoFs) and consistent. By the way, there is no need to fulfill an inf-sup condition. However, standard (symmetric) Nitsche's method includes an extra term that penalizes the boundary/interface conditions and allows to recover stability and optimal accuracy. For this purpose, this extra term makes use of an additional numerical parameter, the *stabilization parameter*, that needs to be fixed above a given threshold. For simple problems and numerical methods, such as piecewise linear or quadratic Lagrange FEM, a direct and accurate estimation of the aforementioned threshold can be effectuated (see, e.g., [45, 44] for a discussion on this topic), but for more realistic problems and less standard numerical methods, this can be harder to achieve. Indeed this threshold for the stabilization will depend upon many parameters, related to the physical constants (Young's modulus) and to the discretization (polynomial order of basis functions, shape of the cells in the grid): see, e.g., [2, 51, 76]. In such situations an alternative to estimate this threshold consists in solving a generalized eigenvalue problem along the target boundary/interface: see, e.g., [45, 44] for FEM and [40, 64, 4] for IGA. Nevertheless, the difficulties associated to this issue can be circumvented by using the penalty-free (skew-symmetric) variant of Nitsche's method, such as in [19, 56, 17, 20, 73].

In this paper we present a simple and systematic procedure to derive, for various boundary and interface conditions, a family of Nitsche's formulations that have different symmetry properties and different degrees of dependency on the stabilization parameter. This family is indexed by the *Nitsche parameter* θ. We then focus on the variant known as the skew-symmetric Nitsche's method, that corresponds to the value $\theta = -1$. This method can be parameter-free when dealing with linear boundary or interface conditions, and reveals to be very robust with respect to the stabilization parameter for non-linear boundary conditions such as contact. Let us mention that in the context of standard FEM, the skew-symmetric method has been successfully applied to contact [25, 23, 27, 24]. Furthermore in IGA there is already one contribution dealing with the skew-symmetric Nitsche's method for enforcing Dirichlet boundary conditions and patch coupling in the context of thin shell problems [43]. In this contribution we perform numerical experiments for different situations, particularly we study how Nitsche's multi-patch coupling can affect the accuracy, the convergence rates, and the condition numbers. Moreover, in modal analysis, literature [30, 21] shows that some outlier frequencies appear due to the discretization of the continuous problem. This "outlier" phenomenon is also captured in multi-patch cases using the mortar method [48]. Here we study this issue

of the "outlier" frequencies and corresponding eigenmodes, in the context of Nitsche's method. Finally to our knowledge Nitsche's method has never been applied in IGA for contact conditions, and we show how to implement Nitsche's formulation for contact problems, and how it performs in these cases.

The outline of this paper is as follows. In Section 2 the concept and notations of IGA are introduced, the critical differences between Lagrange-based FEM and NURBS-based IGA are also explained. In Section 3 we introduce the Nitsche-based formulations for boundary/interface conditions, starting from an abstract setting. In Section 4 various numerical tests are performed and we reach conclusions in Section 5.

2. Brief introduction to isogeometric analysis

Bivariate NURBS basis functions $R_A(\xi,\eta), (A = 1, \cdots, nm)$ are often adopted in IGA to generate surfaces. They are constructed using appropriate weights w_A and the tensor product of two sets of univariate B-spline basis functions $N_{i,p}(\xi), (i = 1, \cdots, n)$ and $N_{j,q}(\eta), (j = 1, \cdots, m)$, where p and q are orders of the B-spline basis functions in directions ξ and η respectively. One set of B-spline basis functions can be calculated from one given knot vector recursively [29]. By the help of NURBS basis functions, the desired surface is represented as the set $\overline{\Omega}$ of points

$$\boldsymbol{x}(\xi,\eta) = \sum_{A=1}^{nm} R_A(\xi,\eta)\, \boldsymbol{x}_A,$$

where $\boldsymbol{x}_A(x,y,z)$ denote positions of the control points. Following the "iso" concept, any (discrete) physical field $\mathbf{u}^h$ defined on the surface (domain) $\overline{\Omega}$ is represented using the same set of NURBS basis functions as

$$\mathbf{u}^h(\xi,\eta) = \sum_{A=1}^{nm} R_A(\xi,\eta)\, \mathbf{u}_A,$$

where $\mathbf{u}_A$ are the control point variables, as well as the degrees of freedom associated to $\mathbf{u}^h$. In the following we will denote by $\mathbf{V}^h$ the finite dimensional space of such discrete fields $\mathbf{u}^h$ constructed using IGA (see, e.g., [11] for the detailed construction of such a space). The notation h will stand for the size of the cells associated to such a discretization. Note that no essential boundary or interface conditions are prescribed in the definition of $\mathbf{V}^h$. According to [86] the spline spaces used for the geometry and the physical field can be chosen and adapted independently, which is known as the Geometry-Independent Field approximaTion (GIFT) and brings more flexibility in the field approximation when preserving geometric exactness and tight CAD integration. However the present research is restricted to IGA.

In Figure (1) some differences between FEM and IGA are illustrated. Consider a contact problem in the left of the figure, and for simplicity we just consider the discretization of a portion of the boundaries that are going into contact. For Lagrange basis function based FEM, discrete errors are introduced by the FEM meshes. For NURBS basis functions based IGA, the curved domain is parametrized exactly. The NURBS basis functions of order p allow to represent fields up to continuity C^{p-1}, however (most) control points that define the boundary/interface are not interpolated, which is owing to the corresponding non-interpolating basis functions. This brings difficulties in directly manipulating the control variables attached to these control points when dealing with boundary and interface conditions. In the next section we are going to introduce Nitsche's formulation to impose various boundary/interface conditions weakly.

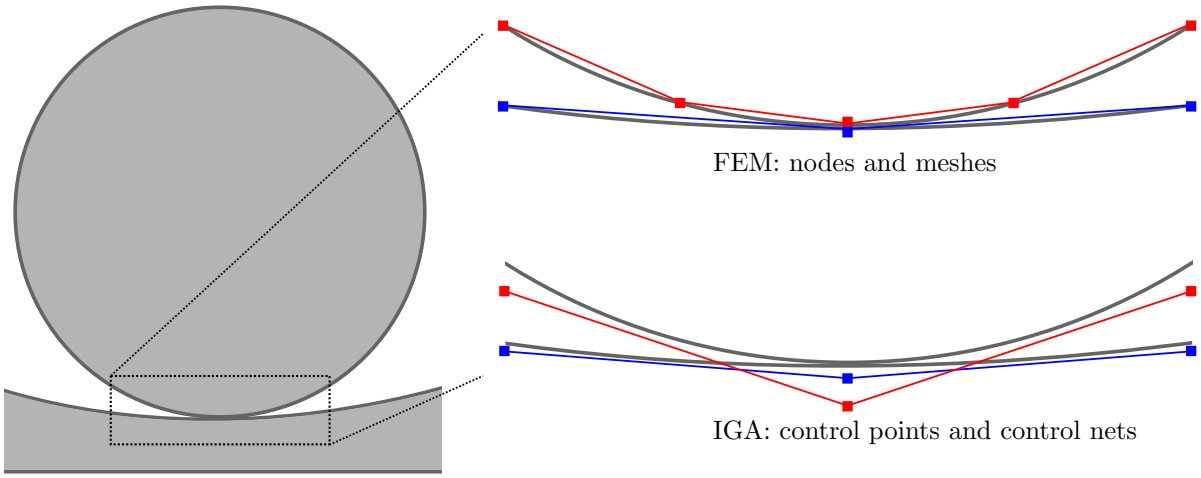

Figure 1: Boundary discretization: Lagrange basis function based FEM and NURBS basis functions based IGA.

3. Nitsche's formulation for boundary/interface conditions

We first present Nitsche's method within an abstract setting, and then show how this framework can be applied to recover various well-known Nitsche-based discretizations, for a wide range of problems in computational mechanics. Note that for linear boundary and interface conditions, discretized with finite elements, a general presentation can be found in, e.g., [79, 9, 44]. We will consider a whole family of Nitsche's methods indexed by a real value, that we will call the *Nitsche parameter* $\theta \in \mathbb{R}$, and we will pay particular attention to the skew-symmetric variant, i.e. to the case $\theta = -1$.

3.1. Abstract setting

Consider the domain Ω as the open set associated to the surface $\overline{\Omega}$ defined in previous Section 2. We will denote by Γ either a portion of the boundary of Ω or an interface that subdivides Ω into two subdomains.

Our aim is to compute a field $\mathbf{u} : \Omega \to \mathbb{R}^d$ ($d \geq 1$), for instance a displacement field, that is a solution to a given set of partial differential equations with prescribed boundary/interface conditions. To simplify the presentation we consider a linear partial differential equation (but not necessarily linear boundary or interface conditions). We will denote by $\mathbf{v}$ an arbitrary test function, that can represent the virtual displacement. Two main ingredients are necessary to build a Nitsche-based formulation.

The first ingredient is a Green formula (inspired by Theorem 5.8 in [54]), that allows to rewrite weakly the partial differential equation satisfied by $\mathbf{u}$, and that we provide below in an abstract setting:

$$\text{Find } \mathbf{u} \in \mathbf{V} \,:\, a(\mathbf{u},\mathbf{v}) - \langle \boldsymbol{\tau}(\mathbf{u}), \mathbf{B}(\mathbf{v}) \rangle_\Gamma = L(\mathbf{v}), \quad \forall\, \mathbf{v} \in \mathbf{V}, \tag{1}$$

where $\mathbf{V}$ is a functional space of admissible fields, $a(\cdot\,,\cdot)$ is a bilinear form (the internal work), $\langle \cdot\,, \cdot \rangle_\Gamma$ is an appropriate duality product for functions on Γ (the boundary/interface work), and $L(\cdot)$ a linear form (the work of external loads). The linear operator $\mathbf{B}$ is a trace-like operator: for instance $\mathbf{B}(\mathbf{v})$ can be the value of $\mathbf{v}$ on Γ, or of its normal component if $\mathbf{v}$ is a vector field. The dual quantity $\boldsymbol{\tau}(\mathbf{u})$, where $\boldsymbol{\tau}$ is a flux-like operator, is to be defined for each situation. It is generaly related to the boundary/interface stress, if $\mathbf{u}$ is a displacement (generalized stress vector in elasticity). We can call $\boldsymbol{\tau}(\mathbf{u})$ and $\mathbf{B}(\mathbf{v})$ a *conjugate pair*. We suppose that both $\boldsymbol{\tau}(\mathbf{u})$ and $\mathbf{B}(\mathbf{v})$ can be represented at almost every point of the boundary as vectors of dimension k ($1 \leq k \leq d$):

$$\boldsymbol{\tau}(\mathbf{u}) : \Gamma \to \mathbb{R}^k, \quad \mathbf{B}(\mathbf{v}) : \Gamma \to \mathbb{R}^k.$$

The second ingredient is a reformulation of the boundary/interface conditions as follows:

$$\boldsymbol{\tau}(\mathbf{u}) = \left[\boldsymbol{\tau}(\mathbf{u}) - \gamma(\mathbf{B}(\mathbf{u}) - \bar{\mathbf{B}}) \right]_S . \tag{2}$$

In the above formula, $\bar{\mathbf{B}}$ is a known, prescribed, quantity associated to the trace. The notation $[\cdot]_S$ stands for the projection onto S, a closed subset of $\mathbb{R}^k$ of admissible values. The set S can depend on $\mathbf{u}$ in some situations ($S = S(\mathbf{u})$), for instance in the case of Coulomb friction [24, 26, 70], but we omit this dependence to simplify our notations. For simple problems, as those studied in this paper, S is generally a closed convex set, a closed convex cone, or a subspace of $\mathbb{R}^k$. Finally γ is an arbitrary positive and one-to-one Schur operator (interface or boundary stiffness), that transforms a trace into a flux.

Nitsche-based discretizations can be obtained by following the steps we describe below in more detail and which are mathematically valid only for sufficiently smooth fields $\mathbf{u}$ and $\mathbf{v}$:

1. Apply the following decomposition

$$\mathbf{B}(\mathbf{v}) = -\gamma^{-1}\left(\theta\boldsymbol{\tau}(\mathbf{v}) - \gamma\mathbf{B}(\mathbf{v})\right) + \theta\gamma^{-1}\boldsymbol{\tau}(\mathbf{v}).$$

2. Insert it into (1), which yields

$$a(\mathbf{u}\,,\mathbf{v}) - \theta\langle\boldsymbol{\tau}(\mathbf{u}), \gamma^{-1}\boldsymbol{\tau}(\mathbf{v})\rangle_\Gamma + \langle\boldsymbol{\tau}(\mathbf{u}), \gamma^{-1}(\theta\boldsymbol{\tau}(\mathbf{v}) - \gamma\mathbf{B}(\mathbf{v}))\rangle_\Gamma = L(\mathbf{v}).$$

3. Inject condition (2) into the above formula, so as to impose it weakly

$$a(\mathbf{u}\,,\mathbf{v}) - \theta\langle\boldsymbol{\tau}(\mathbf{u}), \gamma^{-1}\boldsymbol{\tau}(\mathbf{v})\rangle_\Gamma + \langle[\boldsymbol{\tau}(\mathbf{u}) - \gamma(\mathbf{B}(\mathbf{u}) - \bar{\mathbf{B}})]_S, \gamma^{-1}(\theta\boldsymbol{\tau}(\mathbf{v}) - \gamma\mathbf{B}(\mathbf{v}))\rangle_\Gamma = L(\mathbf{v}). \tag{3}$$

The above formula may have no meaning at the continuous level. Nevertheless it becomes meaningful once all the fields are discretized. For this purpose, consider $\mathbf{V}^h$, a discrete space, built from any Galerkin approximation, such as finite elements or IGA (see Section 2 above). For discrete fields the duality pairing $\langle\cdot,\cdot\rangle_\Gamma$ becomes simply the scalar product in $L^2(\Gamma)$, and we will denote by $\|\cdot\|_{L^2(\Gamma)} (= \langle\cdot,\cdot\rangle_\Gamma^{\frac{1}{2}})$ the corresponding norm. Let us consider

$$\gamma_h : L^2(\Gamma) \to L^2(\Gamma)$$

a discrete Schur operator, positive and one-to-one. Consider $\mathbf{u}^h$ (resp. $\mathbf{v}^h$) a discrete approximation to $\mathbf{u}$ (resp. to $\mathbf{v}$). To simplify the notations, we introduce also the modified discrete weak form

$$\mathrm{A}_\theta(\mathbf{u}^h, \mathbf{v}^h) := a(\mathbf{u}^h, \mathbf{v}^h) - \theta\langle\boldsymbol{\tau}(\mathbf{u}^h), \gamma_h^{-1}\boldsymbol{\tau}(\mathbf{v}^h)\rangle_\Gamma,$$

and the linear operator

$$\mathrm{P}_\theta(\mathbf{v}^h) := \theta\boldsymbol{\tau}(\mathbf{v}^h) - \gamma_h\mathbf{B}(\mathbf{v}^h).$$

Then we obtain the Nitsche-based formulation below

$$\text{Find } \mathbf{u}^h \in \mathbf{V}^h \,:\, \mathrm{A}_\theta(\mathbf{u}^h, \mathbf{v}^h) + \langle[\mathrm{P}_1(\mathbf{u}^h) + \gamma_h\bar{\mathbf{B}}]_S, \gamma_h^{-1}\mathrm{P}_\theta(\mathbf{v}^h)\rangle_\Gamma = L(\mathbf{v}^h), \quad \forall\, \mathbf{v}^h \in \mathbf{V}^h. \tag{4}$$

Remark that the way the method is built ensures its consistency with respect to the partial differential equation being solved.

An important particular case is that of linear boundary/interface conditions, which means that $S = \mathbb{R}^k$

in (2) and so the projection operator is merely the identity. Then (4) reads

$$\mathrm{A}_\theta(\mathbf{u}^h,\mathbf{v}^h)+\langle \mathrm{P}_1(\mathbf{u}^h)+\gamma_h\bar{\mathbf{B}},\gamma_h^{-1}\mathrm{P}_\theta(\mathbf{v}^h)\rangle_\Gamma = L(\mathbf{v}^h),$$

and, after re-ordering and simplifications we arrive at

$$\begin{aligned} & a(\mathbf{u}^h,\mathbf{v}^h)-\langle\boldsymbol{\tau}(\mathbf{u}^h),\mathbf{B}(\mathbf{v}^h)\rangle_\Gamma-\theta\langle\boldsymbol{\tau}(\mathbf{v}^h),\mathbf{B}(\mathbf{u}^h)\rangle_\Gamma+\langle\gamma_h\mathbf{B}(\mathbf{u}^h),\mathbf{B}(\mathbf{v}^h)\rangle_\Gamma \\ = \quad & L(\mathbf{v}^h)-\langle\theta\boldsymbol{\tau}(\mathbf{v}^h)-\gamma_h\mathbf{B}(\mathbf{v}^h),\bar{\mathbf{B}}\rangle_\Gamma. \end{aligned} \tag{5}$$

When $\theta=1$, we recover the well-known formulation presented for instance in [79, 9, 44].

Remark 1. *The Nitsche parameter θ allows to select some variants of Nitsche's formulation, that yield different theoretical properties and different degrees of dependency w.r.t. the operator γ_h:*

- *for $\theta=1$, the standard symmetric Nitsche's method [67] is obtained. If, $a(\cdot,\cdot)$ is symmetric, and under appropriate assumptions on S (for instance if $k=1$ and $S=\mathbb{R}$, $S=\mathbb{R}^-$ or $S=\mathbb{R}^+$), it can be derived as the first order optimality condition of the energy functional [67, 24, 28]:*

$$\mathcal{J}_\mathrm{N}(\mathbf{u}^h):=\frac{1}{2}\mathrm{A}_1(\mathbf{u}^h,\mathbf{u}^h)-L(\mathbf{u}^h)+\frac{1}{2}\langle[\mathrm{P}_1(\mathbf{u}^h)+\gamma_h\bar{\mathbf{B}}]_S,\gamma_h^{-1}[\mathrm{P}_1(\mathbf{u}^h)+\gamma_h\bar{\mathbf{B}}]_S\rangle_\Gamma.$$

  Moreover a suitable choice for γ_h is necessary in order to recover well-posedness and optimal accuracy (see Section 3.2 below);

- *for $\theta=0$, some terms cancel out and we obtain the simple formulation*

$$a(\mathbf{u}^h,\mathbf{v}^h)-\langle[P_1(\mathbf{u}^h)+\gamma_h\bar{\mathbf{B}}]_S,\mathbf{B}(\mathbf{v}^h)\rangle_\Gamma = L(\mathbf{v}^h),$$

  which is close to an augmented lagrangian formulation and easier to extend to the large strain framework [61];

- *for $\theta=-1$, the skew-symmetric Nitsche's method is obtained, see e.g., [41, 19, 17] for linear boundary conditions and [27, 24] for contact conditions. Stability and optimal convergence are ensured whatever γ_h. Note that for linear boundary/interface conditions, we can even choose $\gamma_h=0$, resulting in the*

parameter-free formulation:

$$a(\mathbf{u}^h, \mathbf{v}^h) - \langle \boldsymbol{\tau}(\mathbf{u}^h), \mathbf{B}(\mathbf{v}^h) \rangle_\Gamma + \langle \boldsymbol{\tau}(\mathbf{v}^h), \mathbf{B}(\mathbf{u}^h) \rangle_\Gamma = L(\mathbf{v}^h) + \langle \boldsymbol{\tau}(\mathbf{v}^h), \bar{\mathbf{B}} \rangle_\Gamma. \tag{6}$$

3.2. The discrete Schur operator, well-posedness and optimal accuracy

When $\theta \neq -1$, the discrete Schur operator γ_h needs to be designed so as to preserve well-posedness of Problem (4) as well as optimal accuracy. Let us first consider a linear setting, i.e. Problem (5) and $\theta = 1$: the key issue in the mathematical analysis (see, e.g., [83, 24]) is to ensure the $\mathbf{V}^h$-ellipticity of the bilinear form $\mathrm{A}_1(\cdot\,,\cdot)$ in the energy norm. To this purpose, we define

$$C_{\mathrm{TI}}(h) := \sup_{\mathbf{v}^h \in \mathbf{V}^h} \frac{\|\boldsymbol{\tau}(\mathbf{v}^h)\|^2_{L^2(\Gamma)}}{a(\mathbf{v}^h, \mathbf{v}^h)} \tag{7}$$

the *trace-inverse* constant associated to (5), that depends on the size h of the cells, but also on the other features of the discrete space $\mathbf{V}^h$, such as the polynomial order of basis functions. This constant depends also upon the partial differential equation under consideration (for instance it depends on the Young's modulus in isotropic linear elasticity). Suppose that, for instance, γ_h is such that

$$\|\gamma_h^{-1}\| C_{\mathrm{TI}}(h) \leq \frac{1}{2} \tag{8}$$

with $\|\gamma_h^{-1}\| = \sup_{\tau \in L^2(\Gamma), \|\tau\|_{L^2(\Gamma)}=1} \|\gamma_h^{-1}\tau\|_{L^2(\Gamma)}$. For any $\mathbf{v}^h \in \mathbf{V}^h$, we can write

$$\begin{aligned} \mathrm{A}_1(\mathbf{v}^h, \mathbf{v}^h) &\geq a(\mathbf{v}^h, \mathbf{v}^h) - \|\gamma_h^{-1}\| \|\boldsymbol{\tau}(\mathbf{v}^h)\|^2_{L^2(\Gamma)} \\ &\geq \big(1 - \|\gamma_h^{-1}\| C_{\mathrm{TI}}(h)\big)\, a(\mathbf{v}^h, \mathbf{v}^h) \geq \frac{1}{2} a(\mathbf{v}^h, \mathbf{v}^h). \end{aligned}$$

The same kind of argument holds for the general formulation (4) and for any value of $\theta \neq -1$ (see, e.g., [24] in the case of small strain elasticity with contact). For simple situations, as considered in this paper, where the coefficients of the partial differential equation are constant, and where the mesh is quasi-uniform, the simplest choice is to define the Schur operator globally as

$$\gamma_h := \gamma_0 \, \mathbf{Id}$$

where $\gamma_0 > 0$ is a real parameter, the *stabilization* parameter, and $\mathbf{Id}$ is the identity in $L^2(\Gamma)$. Then condition (8) is reformulated as

$$\gamma_0 \geq 2C_{\mathrm{TI}}(h).$$

As in [40, 64, 4] the constant $C_{\mathrm{TI}}(h)$ can be estimated as the maximum eigenvalue $\lambda^{h,\mathrm{MAX}}$ associated to the problem

$$\text{Find } (\lambda^h, \mathbf{u}^h) \in \mathbb{R} \times \mathbf{V}^h \ : \ \langle \boldsymbol{\tau}(\mathbf{u}^h), \boldsymbol{\tau}(\mathbf{v}^h) \rangle_\Gamma = \lambda^h \, a(\mathbf{u}^h, \mathbf{v}^h) \quad \forall \, \mathbf{v}^h \in \mathbf{V}^h, \tag{9}$$

and then one can choose $\gamma_0 = 2\lambda^{h,\mathrm{MAX}}$. This is actually what we do in the numerical experiments of Section 4.

Of course, if more general situations need to be considered, such as more general (non quasi-uniform) meshes or partial differential equations with spatially variable coefficients, it is much better to consider a local, cell-wise, definition of γ_h: in this case it is chosen piecewise constant on each mesh cell K and a local counterpart of (9) can be solved to recover the value of $\gamma_h|_K$ (see, e.g., [45, 44] in the context of FEM).

In case where $\theta \neq -1$, and in the context of Lagrange FEM, provided that a condition such as (8) is satisfied, both stability and optimal accuracy in the energy norm can be established: see, e.g., [79, 83, 9, 44] for the complete mathematical analysis in the linear setting, and [27, 24] for unilateral contact with Tresca Friction. Moreover standard scaling arguments show that the constant $C_{\mathrm{TI}}(h)$ scales as $\mathcal{O}(h^{-1})$, irrespectively of the polynomial order of the FEM [83]. In the skew-symmetric case $\theta = -1$, the condition (8) can be relaxed, and it suffices to take $\gamma_0 > 0$, or even $\gamma_0 = 0$ for linear boundary/interface conditions ("penalty-free" variant). A complete mathematical analysis for $(\theta, \gamma_0) = (-1, 0)$ can be found in, e.g., [19] for Poisson's problem and in [17] for compressible and incompressible elasticity. The same results as above can be expected for the IGA setting though no numerical analysis has been provided to the best of our knowledge.

In the remaining part of this paper, we will focus on the skew-symmetric variant $\theta = -1$, but numerical tests with the symmetric variant $\theta = 1$ are also performed for comparison purposes.

3.3. Nitsche's formulation for linear boundary conditions

We first illustrate how the above framework can be applied to deal with some linear boundary conditions, thus we consider the case where Γ is a subset of $\partial\Omega$. The unit normal vector on Γ pointing outward of Ω is denoted by $\boldsymbol{n}$.

3.3.1. Dirichlet boundary conditions in small strain elasticity

Consider a linear elastic body described by a small strain constitutive model, that is subjected to body forces $\boldsymbol{b}$, and surface loads $\bar{\boldsymbol{t}}$ along a Neumann boundary $\Gamma_N \subset \partial\Omega$. The corresponding governing equations read

$$\begin{aligned} -\nabla \cdot \boldsymbol{\sigma}(\mathbf{u}) &= \boldsymbol{b} \qquad \text{in } \Omega, \\ \boldsymbol{\sigma}(\mathbf{u})\boldsymbol{n} &= \bar{\boldsymbol{t}} \qquad \text{on } \Gamma_N, \end{aligned} \tag{10}$$

where $\mathbf{u}$ is the unknown displacement field, $\nabla\cdot$ is the divergence operator for vector-valued functions, and $\boldsymbol{\sigma}$ is the Cauchy stress tensor. For the sake of simplicity, we choose to model the elastic behavior using Hooke's law and we denote by E the Young's modulus and by ν the Poisson's ratio. The corresponding weak form reads

$$a(\mathbf{u}\,,\mathbf{v}) - \int_\Gamma \boldsymbol{\sigma}(\mathbf{u})\boldsymbol{n}\cdot\mathbf{v}\,ds = L(\mathbf{v}), \tag{11}$$

where

$$a(\mathbf{u}\,,\mathbf{v}) := \int_\Omega \boldsymbol{\sigma}(\mathbf{u}) : \boldsymbol{\epsilon}(\mathbf{v})\,d\mathbf{x}, \quad L(\mathbf{v}) := \int_\Omega \mathbf{b}\cdot\mathbf{v}\,d\mathbf{x} + \int_{\Gamma_N} \bar{\mathbf{t}}\cdot\mathbf{v}\,ds, \tag{12}$$

and where $\boldsymbol{\epsilon}(\cdot)$ is the small strain tensor. The above formula (11) matches with the general Green formula (1). As illustrated Figure 2, we impose an essential boundary condition on Γ:

$$\mathbf{u} = \bar{\mathbf{u}} \qquad \text{on } \Gamma,$$

where $\bar{\mathbf{u}}$ is the prescribed displacement.

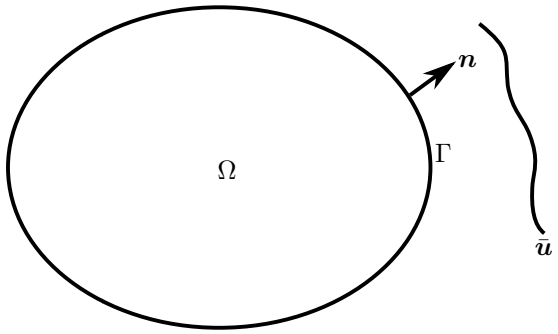

Figure 2: Dirichlet boundary condition: the displacement is equal to $\bar{\mathbf{u}}$ on Γ.

With the choice

$$\mathbf{B}(\mathbf{u}) = \mathbf{u}, \quad \boldsymbol{\tau}(\mathbf{u}) = \boldsymbol{\sigma}(\mathbf{u})\boldsymbol{n}, \quad \bar{\mathbf{B}} = \bar{\mathbf{u}}, \quad S = \mathbb{R}^d,$$

we obtain from (5) the following Nitsche-based formulation

$$\begin{aligned} & \text{Find } \mathbf{u}^h \in \mathbf{V}^h \ : \\ & a(\mathbf{u}^h, \mathbf{v}^h) - \int_\Gamma \big(\boldsymbol{\sigma}(\mathbf{u}^h)\boldsymbol{n}\big) \cdot \mathbf{v}^h \, ds - \theta \int_\Gamma \mathbf{u}^h \cdot \big(\boldsymbol{\sigma}(\mathbf{v}^h)\boldsymbol{n}\big) \, ds + \int_\Gamma \gamma_h \, \mathbf{u}^h \cdot \mathbf{v}^h \, ds \\ = \quad & L(\mathbf{v}^h) - \theta \int_\Gamma \bar{\mathbf{u}} \cdot \big(\boldsymbol{\sigma}(\mathbf{v}^h)\boldsymbol{n}\big) \, ds + \int_\Gamma \gamma_h \, \bar{\mathbf{u}} \cdot \mathbf{v}^h \, ds, \quad \forall \, \mathbf{v}^h \in \mathbf{V}^h. \end{aligned} \tag{13}$$

Setting $\theta = -1$ and $\gamma_h = 0$, the penalty-free variant [19, 71, 17] is recovered.

3.3.2. Symmetry conditions for Kirchhoff-Love plate

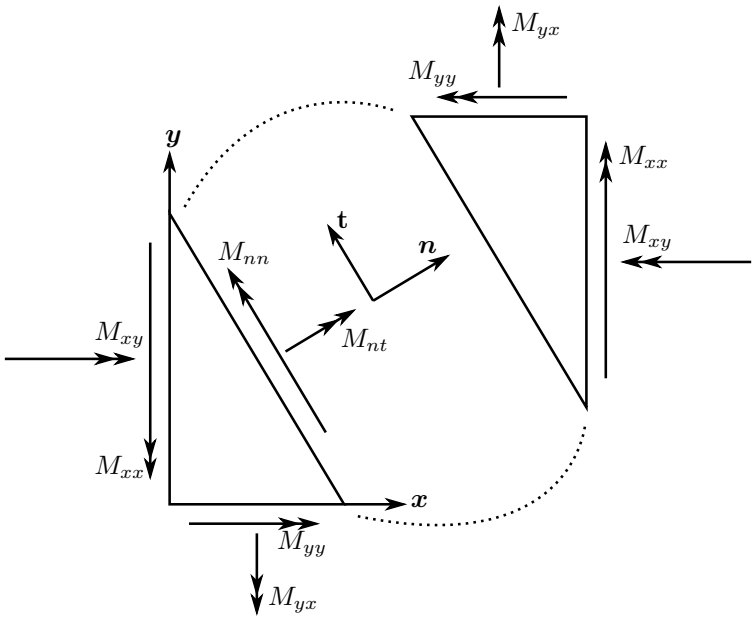

Figure 3: The directions of bending moments in Cartesian coordinate system $(\boldsymbol{x}, \boldsymbol{y})$ and local system $(\boldsymbol{n}, \mathbf{t})$.

Thanks to the higher order continuity properties of NURBS basis functions, there is a regained interest to discretize thin-walled structures using Kirchhoff-Love theory. However due to the absence of rotational degrees of freedom, additional effort is needed to apply rotational boundary conditions. For this fourth-order problem, it is convenient to express the variables in local coordinates, as illustrated in Figure (3). Also, the corresponding weak form for Kirchhoff-Love plates reads

$$a(u, v) - \int_\Gamma M_{nn}(u)(-v_{,n}) \, ds = L(v), \tag{14}$$

where u is the deflection and v the corresponding virtual quantity, $\boldsymbol{n}$ and $\mathbf{t}$ indicate the outward normal

direction and tangential direction respectively, $M_{nn}(u)$ is the normal component of the moment tensor ($\boldsymbol{M}(u) := -\mathcal{C} : \nabla^2 u$, where $\mathcal{C}$ is the constitutive fourth-order tensor) and $v_{,n} := (\nabla v) \cdot \boldsymbol{n}$. In this case the bilinear and linear form read (see, e.g., [47] for a more general formulation)

$$a(u,v) := -\int_\Omega \boldsymbol{M}(u) : (\nabla^2 v)\, d\mathbf{x}, \quad L(v) := \int_\Omega f\, v\, d\mathbf{x},$$

with f a distributed load. The symmetry condition on the boundary Γ is formulated using the normal derivative of the mid-surface deflection u. More specifically, we impose:

$$-u_{,n} = \bar{\theta}_t \qquad \text{on } \Gamma,$$

where $\bar{\theta}_t$ is a prescribed rotation. Recall that Nitsche's contributions use *conjugate pairs*: in this case these are the rotation and the corresponding bending moment. In order to form the Nitsche's contribution the rotation direction should be consistent with the direction of the corresponding bending moment (see Figure (3)).

With the choice

$$\mathbf{B}(\mathbf{u}) = -u_{,n}, \quad \boldsymbol{\tau}(\mathbf{u}) = M_{nn}(u), \quad \bar{\mathbf{B}} = \bar{\theta}_t, \quad S = \mathbb{R},$$

the Nitsche-based formulation is derived from (5) (see as well [40, 47, 73]):

$$\begin{aligned} &\text{Find } u^h \in V^h \ : \\ &a(u^h, v^h) - \int_\Gamma M_{nn}(u^h)\left(-v^h_{,n}\right)\, ds - \theta \int_\Gamma \left(-u^h_{,n}\right) M_{nn}(v^h)\, ds + \int_\Gamma \gamma_h \left(-u^h_{,n}\right)\left(-v^h_{,n}\right)\, ds \\ &= L(v^h) - \theta \int_\Gamma \bar{\theta}_t M_{nn}(v^h)\, ds + \int_\Gamma \gamma_h \bar{\theta}_t \left(v^h_{,n}\right)\, ds, \quad \forall\, v^h \in V^h. \end{aligned} \tag{15}$$

As previously, we recover a penalty-free method by setting $\theta = -1$, $\gamma_h = 0$.

3.4. Nitsche's formulation for interface conditions and patch coupling

Consider now an interface problem in which the domain Ω is decomposed into two sub-domains Ω^m (see Figure (4)), where the superscript $m = 1, 2$ is used to mark the partitioned domain and the corresponding variables. The shared boundary between Ω^1 and Ω^2 is denoted by Γ, and $\boldsymbol{n}^m$ is the unit normal along the interface Γ, pointing out of Ω^m. We still consider elasticity equations in small strains, and search for a

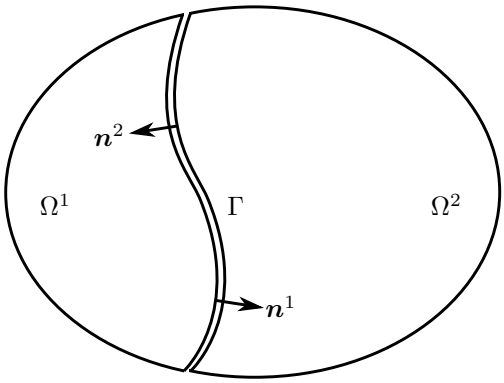

Figure 4: Problem with decomposed continuum domain. Domain Ω is decomposed into two sub-domains Ω^1 and Ω^2. The shared boundary is denoted by Γ along which the outward unit normals are denoted by $\boldsymbol{n}^m$, $m = 1, 2$.

displacement field $\mathbf{u} = (\mathbf{u}^1, \mathbf{u}^2)$ solution to

$$\begin{aligned} -\nabla \cdot \boldsymbol{\sigma}(\mathbf{u}^m) &= \boldsymbol{b}^m \qquad \text{in } \Omega^m, \\ \boldsymbol{\sigma}(\mathbf{u}^m)\boldsymbol{n}^m &= \bar{\boldsymbol{t}}^m \qquad \text{on } \Gamma_N^m, \\ \mathbf{u}^m &= \mathbf{0} \qquad \text{on } \Gamma_D^m, \end{aligned}$$

If Dirichlet boundary conditions on Γ_D^m are non-homogeneous, they can be, for instance, treated as in Section 3.3.1 (but we omit this point to simplify notations). In addition, there holds the following interface conditions

$$\begin{aligned} \mathbf{u}^1 - \mathbf{u}^2 &= \mathbf{0} \qquad \text{on } \Gamma, \\ \boldsymbol{\sigma}(\mathbf{u}^1)\boldsymbol{n}^1 + \boldsymbol{\sigma}(\mathbf{u}^2)\boldsymbol{n}^2 &= \mathbf{0} \qquad \text{on } \Gamma. \end{aligned}$$

The first equation corresponds to the continuity of the displacement along the interface, while the second one is the action-reaction principle. Note that this situation corresponds both to interface problems (when, for instance, material properties are different in Ω_1 and Ω_2) and to patch coupling (where the interface between subdomains is artificial, as in [64]).

Let us define the jump and average operators along the interface Γ

$$\begin{aligned} [\![\mathbf{u}]\!] &:= \mathbf{u}^1 - \mathbf{u}^2, \\ \langle \boldsymbol{\sigma}(\mathbf{u}) \rangle &:= \frac{1}{2}(\boldsymbol{\sigma}(\mathbf{u}^1)\boldsymbol{n}^1 - \boldsymbol{\sigma}(\mathbf{u}^2)\boldsymbol{n}^2). \end{aligned}$$

Let us introduce also

$$
\begin{aligned}
a(\mathbf{u}\,,\mathbf{v}) &:= \sum_{m=1}^{2} \int_{\Omega^m} \boldsymbol{\sigma}^m(\mathbf{u}^m) : \boldsymbol{\epsilon}^m\left(\mathbf{v}^m\right)\, d\mathbf{x}, \\
L(\mathbf{v}) &:= \sum_{m=1}^{2} \int_{\Omega^m} \boldsymbol{b}^m \cdot \mathbf{v}^m \, d\mathbf{x} + \sum_{m=1}^{2} \int_{\Gamma_N^m} \bar{\boldsymbol{t}}^m \cdot \mathbf{v}^m \, ds.
\end{aligned}
\tag{16}
$$

Green formula for elasticity equations yields

$$
a(\mathbf{u}\,,\mathbf{v}) - \int_\Gamma (\boldsymbol{\sigma}(\mathbf{u}^1)\boldsymbol{n}^1)\cdot \mathbf{v}^1 \, ds - \int_\Gamma (\boldsymbol{\sigma}(\mathbf{u}^2)\boldsymbol{n}^2)\cdot \mathbf{v}^2 \, ds = L(\mathbf{v}).
$$

Remark now that the action-reaction principle implies the following identity

$$
\boldsymbol{\sigma}(\mathbf{u}^1)\boldsymbol{n}^1 = \frac{1}{2}\boldsymbol{\sigma}(\mathbf{u}^1)\boldsymbol{n}^1 + \frac{1}{2}\boldsymbol{\sigma}(\mathbf{u}^1)\boldsymbol{n}^1 = \frac{1}{2}\boldsymbol{\sigma}(\mathbf{u}^1)\boldsymbol{n}^1 - \frac{1}{2}\boldsymbol{\sigma}(\mathbf{u}^2)\boldsymbol{n}^2 = \langle\boldsymbol{\sigma}\rangle = -\boldsymbol{\sigma}(\mathbf{u}^2)\boldsymbol{n}^2.
$$

This allows to impose weakly the action-reaction principle, as an essential interface condition, and we obtain the appropriate Green formula in this context, as a particular form of (1):

$$
a(\mathbf{u}\,,\mathbf{v}) - \int_\Gamma \langle\boldsymbol{\sigma}(\mathbf{u})\rangle [\![\mathbf{v}]\!]\, ds = L(\mathbf{v}). \tag{17}
$$

With the choice

$$
\mathbf{B}(\mathbf{u}) = [\![\mathbf{u}]\!], \quad \boldsymbol{\tau}(\mathbf{u}) = \langle\boldsymbol{\sigma}(\mathbf{u})\rangle, \quad \bar{\mathbf{B}} = \mathbf{0}, \quad S = \mathbb{R}^d,
$$

formulation (5) reads:

$$
\begin{aligned}
&\text{Find } \mathbf{u}^h \in \mathbf{V}^h \ : \\
&a(\mathbf{u}^h, \mathbf{v}^h) - \int_\Gamma \langle\boldsymbol{\sigma}(\mathbf{u}^h)\rangle [\![\mathbf{v}^h]\!]\, ds - \theta \int_\Gamma [\![\mathbf{u}^h]\!] \langle\boldsymbol{\sigma}(\mathbf{v}^h)\rangle \, ds + \int_\Gamma \gamma_h \, [\![\mathbf{u}^h]\!][\![\mathbf{v}^h]\!]\, ds = L(\mathbf{v}^h), \quad \forall\, \mathbf{v}^h \in \mathbf{V}^h.
\end{aligned}
\tag{18}
$$

Once again we recover a penalty-free formulation with $\theta = -1$, $\gamma_h = 0$. Note as well that the same technique can be applied for patch coupling between other models, such as plates or rods, with the appropriate changes of notations [65].

3.5. Nitsche's formulation for frictionless contact conditions

In this section we get back to the general (non-linear) formulation (4) and illustrate it in the case of frictionless contact, following [24]. In 3.5.1 we first present Signorini contact and biased (master-slave)

contact, in which the contact conditions are imposed on the boundary of one unique elastic body, in the same fashion as in Section 3.3. For contact between two bodies (or multi-body contact and self-contact), it is more convenient to impose contact conditions on both contact surfaces, using an unbiased formalism, as in, e.g., [72, 28, 61]. So we present in 3.5.2 an unbiased Nitsche's method, that can be derived in the same manner as presented in 3.4 for interface conditions.

We still consider elastic bodies undergoing small strain and governed by Hooke's law, so we keep the same notations as in the previous sections, especially 3.3.1.

3.5.1. Biased frictionless contact conditions

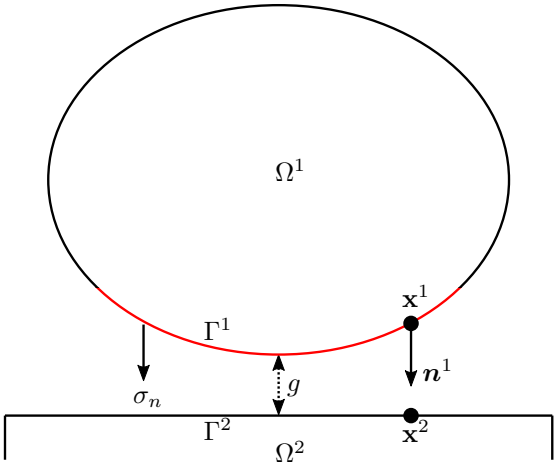

Figure 5: Contact problem setup, the contact slave surface is colored in red.

Consider a contact problem between an elastic body $\Omega := \Omega_1$ and a rigid support Ω_2 as depicted in Figure (5). Surfaces for potential contact are denoted by $\Gamma := \Gamma_1$ and Γ_2. To formulate the non-penetration condition, the normalized vector is introduced

$$\boldsymbol{n}^1 := \frac{\mathbf{x}^2 - \mathbf{x}^1}{||\mathbf{x}^2 - \mathbf{x}^1||},$$

where $\mathbf{x}^1$ and $\mathbf{x}^2$ are two mapped points on the corresponding boundary of each body Ω_1 and Ω_2, for instance $\mathbf{x}^2$ is the orthogonal projection of $\mathbf{x}^1$ on Γ_2. Then the gap function is defined as

$$g := (\mathbf{x}^2 - \mathbf{x}^1) \cdot \boldsymbol{n}^1.$$

We deal with frictionless contact on Γ, so we impose weakly the essential condition $\boldsymbol{\sigma_t}(\mathbf{u}) = \mathbf{0}$, where $\boldsymbol{\sigma_t}$ denotes the tangential stress. We start from equations (10) and we obtain the following Green formula,

which is the counterpart of (11) for Dirichlet boundary conditions:

$$a(\mathbf{u}\,,\mathbf{v}) - \int_\Gamma \sigma_n(\mathbf{u}) v_n \, ds = L(\mathbf{v}), \tag{19}$$

with the expression of $a(\cdot,\cdot)$ and $L(\cdot)$ provided in (12), and where $\sigma_n(\mathbf{u})$ (resp. v_n) is the normal component of the Cauchy stress on the boundary (resp. the normal component of the virtual displacement). The Signorini-type contact conditions (Karush-Kuhn-Tucker conditions) are expressed as (see, e.g., [54])

$$u_n - g \leq 0 \qquad \text{on } \Gamma, \tag{20a}$$

$$\sigma_n(\mathbf{u}) \leq 0 \qquad \text{on } \Gamma, \tag{20b}$$

$$\sigma_n(\mathbf{u})\,(u_n - g) = 0 \qquad \text{on } \Gamma. \tag{20c}$$

Equation (20a) is the non-penetration condition, whereas Equation (20b) means the contact is non-adhesive, and Equation (20c) is the complementarity condition.

With the choice

$$\mathbf{B}(\mathbf{u}) = u_n, \quad \boldsymbol{\tau}(\mathbf{u}) = \sigma_n(\mathbf{u}), \quad \bar{\mathbf{B}} = g, \quad S = \mathbb{R}^-,$$

formulation (4) reads

$$\text{Find } \mathbf{u}^h \in \mathbf{V}^h \,:\, \mathrm{A}_\theta(\mathbf{u}^h, \mathbf{v}^h) + \int_\Gamma \gamma_h^{-1} [\mathrm{P}_1(\mathbf{u}^h) + \gamma_h g]_{\mathbb{R}^-} \, \mathrm{P}_\theta(\mathbf{v}^h) \, ds = L(\mathbf{v}^h), \quad \forall\, \mathbf{v}^h \in \mathbf{V}^h, \tag{21}$$

which is exactly the formulation presented in [27, 24].

Remark 2. *The contact formulation is not parameter-free, and the choice $\gamma_h = 0$ ("penalty-free") is not permitted for contact. However see for instance [20] for a first attempt at deriving a penalty-free method for Signorini contact.*

The adaptation of the above formulation (21) for biased (master-slave) contact between two elastic bodies (see, e.g., [24]), reads:

$$\mathbf{B}(\mathbf{u}) = [\![u]\!]_n^{sl}, \quad \boldsymbol{\tau}(\mathbf{u}) = \sigma_n^{sl}(\mathbf{u}), \quad \bar{\mathbf{B}} = g, \quad S = \mathbb{R}^-,$$

where $[\![u]\!]_n^{sl} := (\mathbf{u}^1(\mathbf{x}^1) - \mathbf{u}^2(\mathbf{x}^2)) \cdot \boldsymbol{n}^1$ is the relative displacement written on the slave surface, and $\sigma_n^{sl}(\mathbf{u})(= \sigma_n(\mathbf{u}^1))$ is the contact pressure on the slave surface. Also the bilinear form $a(\cdot\,,\cdot)$ and the linear form $L(\cdot)$ should incorporate the virtual work of both the master and slave elastic bodies, *i.e.* they should be defined

as in (16) (see, e.g., [24] and references therein for more details).

Remark 3. *The same methodology can be extended to other problems, involving for instance friction, dynamics and large deformations, please refer to [24] for a (non-restrictive) overview of possible extensions.*

Remark 4. *It is generally considered that the Sobolev regularity of contact problems is lower than $H^{\frac{5}{2}}(\Omega)$ in two dimensions, due to weak singularities associated to transitions between binding and non-binding (see, e.g., [62]). This means that, in general, FEM or IGA approximations of order higher than two do not improve the convergence rate in the energy norm, which remains limited to $\mathcal{O}(h^{\frac{3}{2}})$ (see, e.g., [5] in case of quadratic finite elements and, e.g., [3] for IGA). Nevertheless, as discussed in [3] the interest of the IGA approximation for contact is to obtain easily smooth gap functions g, which makes the numerical method more robust. As well, higher order approximations allow to recover smoother contact pressures. To perform better in terms of convergence, higher order approximations need to be combined with adaptive refinement, as in [34, 35, 57].*

3.5.2. Unbiased frictionless contact

Consider now the same situation as in the previous section 3.5.1 and depicted Figure (5), but this time with Ω^1 and Ω^2 that represent both two elastic bodies in frictionless contact. Assume also, for simplicity, that there is no initial gap ($g = 0$). We proceed first the same way as in Section 3.4 and obtain the Green formula (17). We apply the frictionless condition, use the definition of $\langle \boldsymbol{\sigma}(\mathbf{u}) \rangle$, and separate the contributions on the two sides Γ^1 and Γ^2 of the interface, so the Green formula (17) can be re-written equivalently as

$$a(\mathbf{u}, \mathbf{v}) - \frac{1}{2} \int_{\Gamma^1} \sigma_n^1(\mathbf{u}^1) [\![v]\!]_n^1 \, ds - \frac{1}{2} \int_{\Gamma^2} \sigma_n^2(\mathbf{u}^2) [\![v]\!]_n^2 \, ds = L(\mathbf{v}), \tag{22}$$

with the notations $[\![v]\!]_n^1 := (\mathbf{v}^1 - \mathbf{v}^2) \cdot \boldsymbol{n}^1$ and $[\![v]\!]_n^2 := (\mathbf{v}^2 - \mathbf{v}^1) \cdot \boldsymbol{n}^2$. We now apply frictionless contact conditions on the product set $\Gamma_1 \times \Gamma_2$:

$$\mathbf{B}(\mathbf{u}) = ([\![u]\!]_n^1, [\![u]\!]_n^2), \quad \boldsymbol{\tau}(\mathbf{u}) = (\sigma_n(\mathbf{u}^1), \sigma_n(\mathbf{u}^2)), \quad \bar{\mathbf{B}} = (0, 0), \quad S = \mathbb{R}^- \times \mathbb{R}^-.$$

The following unbiased formulation for contact is obtained

$$\text{Find } \mathbf{u}^h \in \mathbf{V}^h \, : \, \mathrm{A}_\theta(\mathbf{u}^h, \mathbf{v}^h) + \frac{1}{2} \sum_{m=1}^{2} \int_{\Gamma^m} (\gamma_h^m)^{-1} \, [\mathrm{P}_1^m(\mathbf{u}^h)]_{\mathbb{R}^-} \, \mathrm{P}_\theta^m(\mathbf{v}^h) \, ds = L(\mathbf{v}^h), \quad \forall \, \mathbf{v}^h \in \mathbf{V}^h, \tag{23}$$

where

$$\mathrm{A}_\theta(\mathbf{u}^h, \mathbf{v}^h) := a(\mathbf{u}^h, \mathbf{v}^h) - \frac{\theta}{2} \sum_{m=1}^{2} \int_{\Gamma^m} (\gamma_h^m)^{-1} \, \sigma_n(\mathbf{u}^{h,m}) \sigma_n(\mathbf{v}^{h,m}) \, ds,$$

with $a(\cdot, \cdot)$ defined as in (16), and, for $m = 1, 2$,

$$\mathrm{P}_\theta^m(\mathbf{v}^h) := \theta \sigma_n(\mathbf{v}^{h,m}) - \gamma_h^m [\![v^h]\!]_n^m.$$

This is a special case of [28] (see [61, 28] for the detailed derivation in a more general setting). Remark that this formulation does not indeed differentiate between a master and a slave surface.

4. Numerical studies

To study the performance of the proposed skew-symmetric Nitsche's method, we present some numerical tests. We consider the IGA setting described in Section 2 with equal order of approximation in all directions, and carry out tests for different orders. To avoid additional errors due to numerical integration, unless otherwise specified, elements with C^{p-1} continuity are adopted for order p, and $p + 1$ Gauss quadrature points are used for each element (and the same applies for other directions). All the methods are implemented within the open source C++ IGA library *Gismo* [1] [52].

We recall that the skew-symmetric Nitsche's method corresponds to the Nitsche parameter $\theta = -1$. For most of the numerical tests, we compare the performance of this method to the symmetric variant, that corresponds to $\theta = 1$, and that will be denominated standard Nitsche's method. In this case the stabilization parameter is determined as $\gamma_0 = 2\lambda^{h,\mathrm{MAX}}$ where $\lambda^{h,\mathrm{MAX}}$ is obtained from (9).

In order to evaluate the performances numerically, the relative errors on the displacement field $\mathbf{u}$ within the domain Ω is computed, in the L^2-norm, denoted by $\| \cdot \|_{L^2(\Omega)}$, and in the energy norm, denoted by $\| \cdot \|_{E(\Omega)} (= \sqrt{\int_\Omega \boldsymbol{\sigma}(\cdot) : \boldsymbol{\epsilon}(\cdot) \, d\mathbf{x}})$.

4.1. Linear boundary conditions

4.1.1. Dirichlet boundary conditions patch test

In this section we focus on the setting presented in 3.3.1 and illustrate the skew-symmetric Nitsche's formulation is able to pass the rectangular patch tests and has optimal convergence rate in energy norm for circular shaped patch tests. In Figure (6) we consider a linear elastic media in a square (resp. circular)

[1] https://ricamsvn.ricam.oeaw.ac.at/trac/gismo/wiki/WikiStart

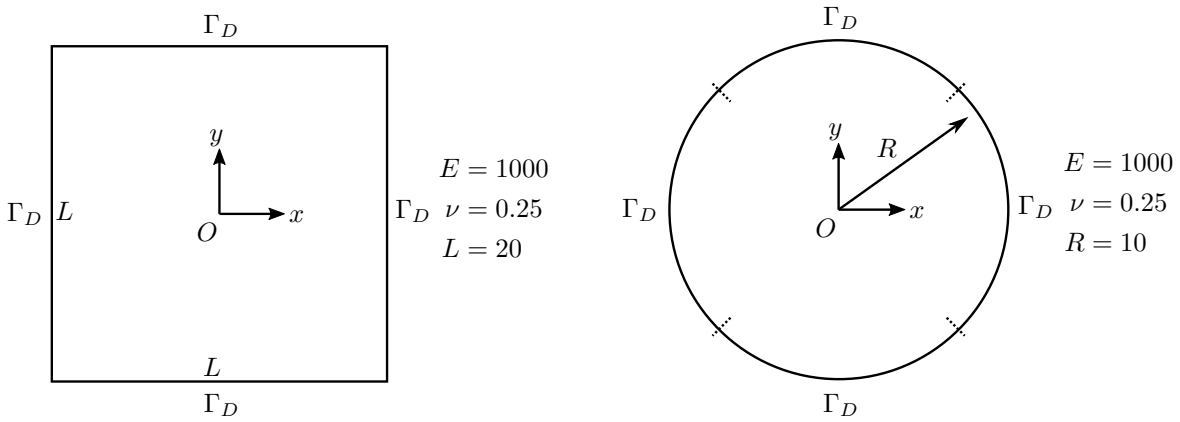

(a) Rectangular patch (b) Circular patch

Figure 6: Patch test problems.

domain Ω of length $L = 20$ (resp. radius $R = 10$), with a Young's modulus $E = 1000$ and a Poisson's ratio $\nu = 0.25$.

The patch test is traditionally adopted to verify the consistency of a newly proposed element. However, in the following, another type of patch test, i.e. the B-type patch test [91], is used to test the effectiveness of the skew-symmetric Nitsche's method in imposing Dirichlet boundary conditions. Firstly we set the exact solution as $\mathbf{u}^{\text{ref}}$, and impose the value $\bar{\mathbf{u}} = \mathbf{u}^{\text{ref}}|_{\Gamma_D}$ on the whole boundary $\Gamma_D := \partial\Omega$ in (10). No external force is imposed: $\boldsymbol{b} = \mathbf{0}$. Finally problem (5) is solved and the corresponding solution $\mathbf{u}^h$ is compared against the exact solution $\mathbf{u}^{\text{ref}}$. In order to fulfill the equilibrium strain condition, an exact solution of displacement field up to fourth order is set up as in [22]:

$$\begin{cases} u_x(x,y) = \frac{1}{4} + x + 3y - 2x^2 - 4xy + \frac{5}{2}y^2 - 2x^3 + x^2y - 4xy^2 - \frac{1}{3}y^3 - \frac{7}{32}x^4 - \frac{19}{24}x^3y + x^2y^2 + xy^3 - \frac{11}{96}y^4, \\ u_y(x,y) = 1 + \frac{1}{2}x + 2y - \frac{2}{3}x^2 + \frac{17}{5}xy + \frac{3}{2}y^2 + \frac{1}{3}x^3 + 12x^2y - xy^2 - \frac{2}{3}y^3 - \frac{11}{96}x^4 + x^3y + x^2y^2 - \frac{19}{24}xy^3 - \frac{7}{32}y^4, \end{cases}$$

where u_x (resp. u_y) is the x-component (resp y-component) of $\mathbf{u}^{\text{ref}}$, truncated to the appropriate order. For example, if the patch test of order one is performed, then the exact solution is truncated as

$$\begin{cases} u_x(x,y) = \frac{1}{4} + x + 3y, \\ u_y(x,y) = 1 + \frac{1}{2}x + 2y. \end{cases}$$

The results of the rectangular patch tests are presented in Table 1, showing that the skew-symmetric Nitsche's method is able to pass the appropriate patch tests of order up to p for $p = 2, 3, 4$. The circular patch tests cannot be passed exactly, because Nitsche's method imposes the boundary constraints weakly. However according to Figure (7) the error in the energy norm is reduced with an optimal convergence rate

Table 1: The skew-symmetric Nitsche's formulation passes (Y) the rectangular patch tests.

Patch test order	1	2	3	4
IGA $p = q = 2$	Y	Y	N	N
IGA $p = q = 3$	Y	Y	Y	N
IGA $p = q = 4$	Y	Y	Y	Y

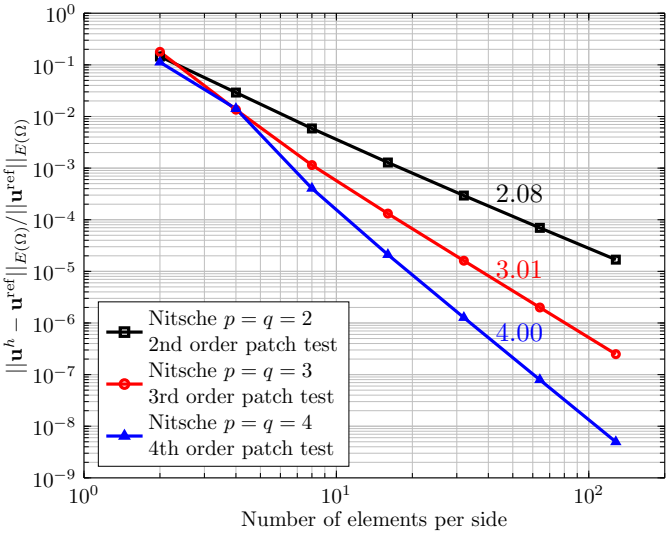

Figure 7: Circular patch test: relative errors of displacement field in energy norm. Skew-symmetric Nitsche's method is used.

of order p, as predicted theoretically for IGA and a conformal setting (i.e. strong imposition of Dirichlet boundary conditions) [8]. This is also in agreement with the observed behavior of skew-symmetric Nitsche's formulation with FEM: see for instance [17] where the same rates are obtained numerically for quadratic finite elements. As regarding the convergence in $L^2(\Omega)$-norm, a sub-optimality of order $\mathcal{O}(h^{\frac{1}{2}})$ is predicted by the theory, due to the lack of adjoint-consistency of skew-symmetric Nitsche's method, but this behavior seems difficult to observe in practical situations (see [17]).

4.1.2. Symmetry conditions for Kirchhoff plates

In this section we illustrate the effectiveness of Nitsche's formulation to handle rotational boundary conditions for Kirchhoff plates, as described in 3.3.2. Figure (8) describes a simply supported thin square plate of thickness t, made of an isotropic elastic material, and subjected to a distributed transverse load f. Figure (8) provides also the values of the model parameters. Due to the symmetry of this problem, only one quarter of the geometry is modeled, where two of the model boundaries are simply supported, and the

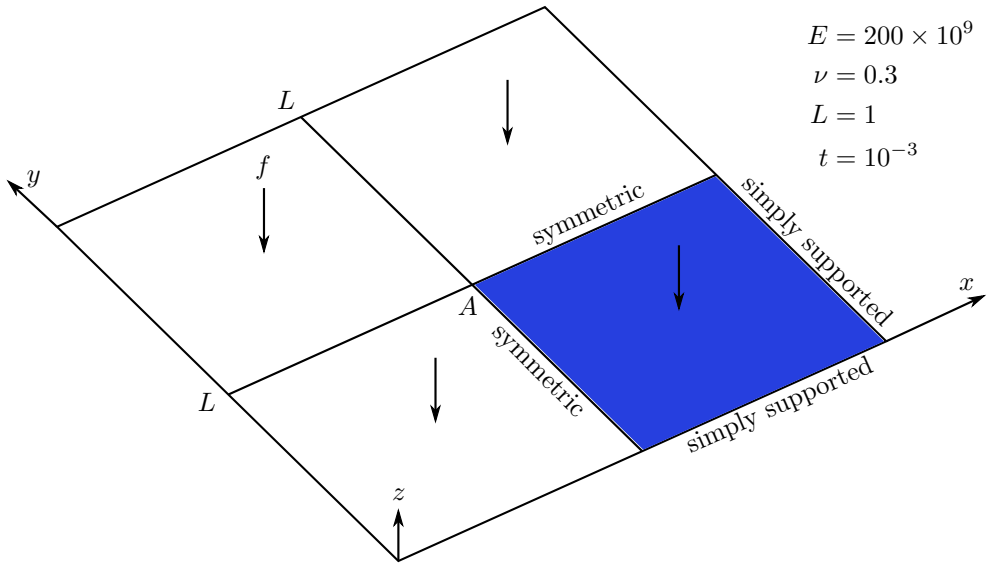

Figure 8: Square thin plate under distributed transverse load, only 1/4 of the plate (blue area) is modeled.

other two require symmetric constraints:

$$\bar{\theta}_t = 0 \qquad \text{on } y = \frac{L}{2} \text{ and } x = \frac{L}{2}.$$

For a sinusoidally distributed transverse load

$$f(x, y) = -10 \sin(\pi x) \sin(\pi y),$$

the analytical solution of the deflection is given by [69]

$$u^{\text{ref}}(x, y) = \frac{-10}{4\pi^4 D} \sin(\pi x) \sin(\pi y),$$

in which $D = \frac{Et^3}{12(1-\nu^2)}$ is the flexural rigidity.

We firstly implement the 'second row' strategy [53] by penalty method for comparison. As illustrated in Figure (9), the idea of the 'second row' strategy consists in enforcing the displacements of the control points along the symmetric boundary and the neighboring row to be equal. This is achieved by adding a penalty coefficient W in the stiffness matrix [2]. However in this way, the convergence results depend significantly on the penalty parameters, and the constraints of the four control points are penalized twice (see Figure (9))

[2] http://www.colorado.edu/engineering/CAS/courses.d/IFEM.d/IFEM.Ch09.d/IFEM.Ch09.pdf

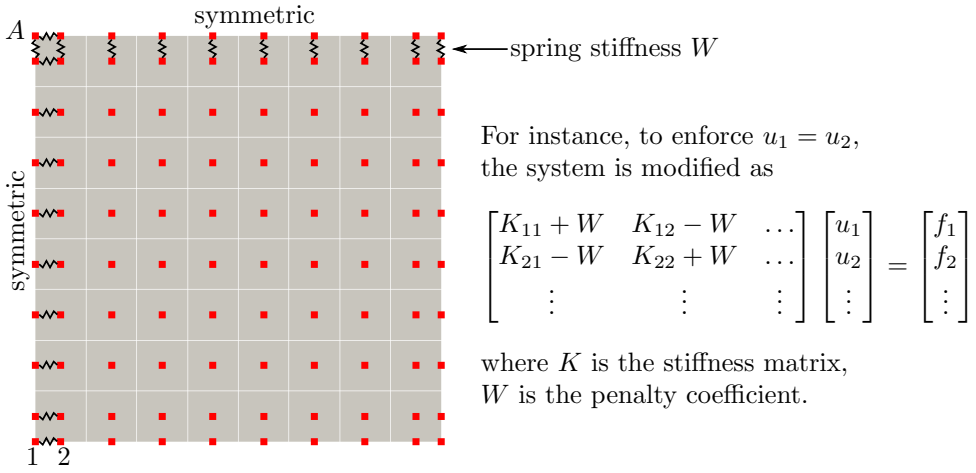

Figure 9: The 'second row' strategy with penalty method to impose the symmetry boundary conditions. The four control points near point A are penalized twice.

near the corner point A, which makes the corner deflection even more sensitive to the penalty coefficient. The results using different penalty parameters are shown in Figure (10) (a). It is concluded that a suitable value of the penalty parameter W should be chosen carefully for different meshes and orders.

The results obtained by Nitsche's method are shown in Figure (10) (b). The stabilization parameter γ_0 for the standard (symmetric) Nitsche's formulation is acquired by solving the generalized eigenvalue problem (9). Remember that the Kirchhoff problem results in a fourth order system with respect to the deflection u, the strain $\boldsymbol{\epsilon}$ consists of second order derivatives of u, thus the "energy norm" in this situation is equivalent to the H^2 semi-norm on the deflection, and the optimal convergence rate is expected to be $p-1$ in the energy norm for approximation order p [40]. As indicated in Figure (10) (b), for relative errors in energy norm the skew-symmetric Nitsche's method and the standard one are similar, and both standard and skew-symmetric Nitsche's formulations converge optimally with the expected orders associated to Kirchhoff plate theory.

4.2. Linear interface conditions and patch coupling

4.2.1. Patch coupling effects: statics

In this section, we study whether additional effects are introduced into the accuracy, convergence performance and condition numbers when a patch coupling in statics is performed by Nitsche's method. The problem setup is shown in Figure (11): in the left figure we present a plate model with thickness $t = 10^{-1}$, Young's modulus $E = 200 \times 10^9$ and Poisson's ratio $\nu = 0.3$. The plate is subjected to uniform pressure f with four edges being simply supported. In the right figure the domain Ω is artificially broken into two identical patches Ω_1 and Ω_2. It corresponds then to the setting described in 3.4 with the value of the parameters provided in Figure (11), and with an approximation using degenerate Reissner-Mindlin elements,

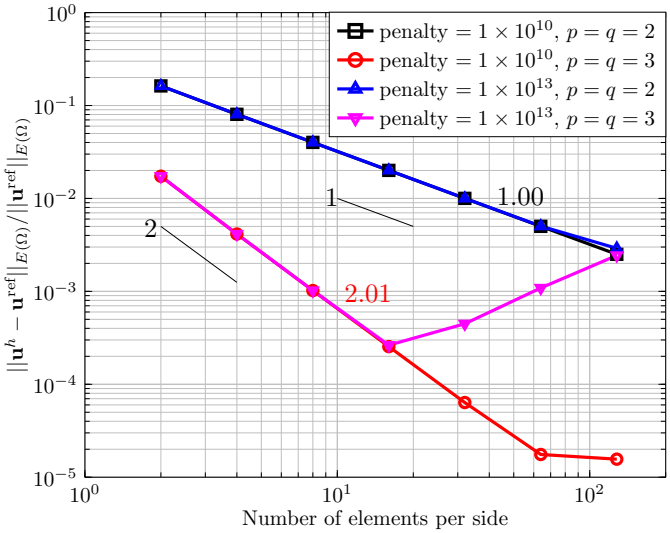

(a) The 'second row' strategy using penalty method

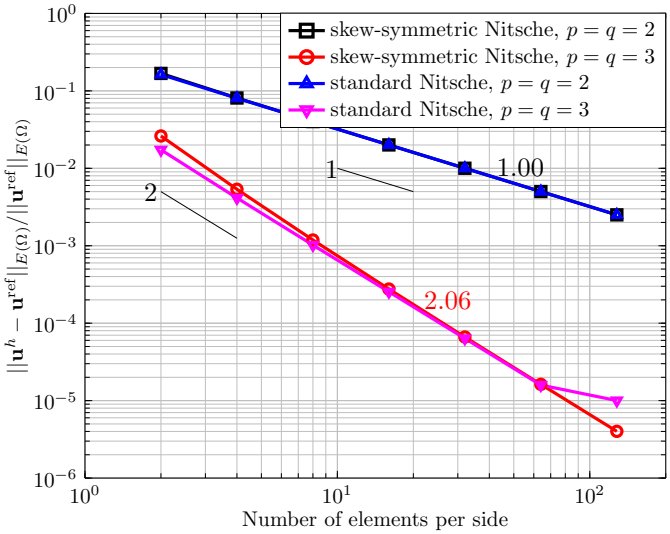

(b) Nitsche's method

Figure 10: Kirchhoff plate: relative errors of deflection field in energy norm. Symmetric rotational boundary conditions are imposed by the 'second row' strategy using penalty method (a), and Nitsche's method (b).

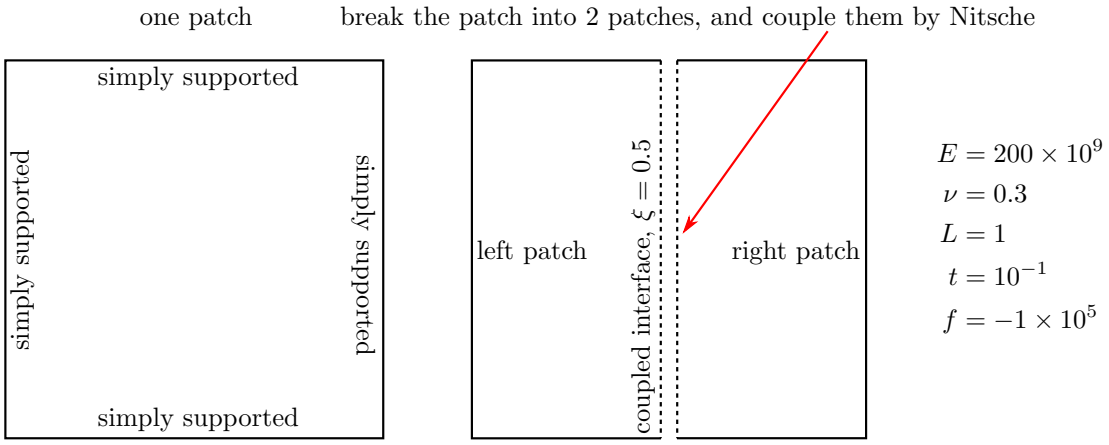

Figure 11: Plate model with four simply supported edges. On the left, one patch model is adopted as the control group. On the right, the plate is artificially broken into two conforming patches and the interface is coupled by Nitsche's method.

in which only the mid-surface of the plate has to be modeled [1]. The deflection field approximated with (conforming) IGA using one patch of 1,024 elements of order $p(= q) = 5$ is adopted as the reference.

We compare symmetric and skew-symmetric variants of Nitsche's method, and for the symmetric variant, we still compute γ_0 by solving the generalized eigenvalue problem (9). The convergence performance is plotted in Figure (12). In this test the meshes of the left patch and the right patch are equal (for instance, for conforming patch the mesh is 8×8, then for two patch coupling the meshes are 4×8 and 4×8 for the left patch and right patch respectively), in order to evaluate the coupling influence on the approximation of the displacement. By artificially breaking the patch into two patches and couple them by Nitsche's method, the obtained errors is to some degrees different from the one patch case. Skew-symmetric and standard formulations perform very similarly, and as we refine the mesh, both converge with nearly optimal rates.

The condition numbers of the obtained stiffness matrix are given in Table (2). From a general viewpoint, h-refinement of the mesh, which means that using more control points, increases the corresponding condition number. It is noticed that the condition number obtained from Nitsche's coupling is larger than one patch IGA. This is inferred to be related to the coupling effects. Specifically, the skew-symmetric Nitsche's formulation slightly increases the condition number compared to conforming IGA because there are more control points along the coupled interface, moreover the condition numbers are almost independent of the mesh size h and basis functions orders p and q. The standard Nitsche's formulation increases the condition number significantly, because of the large value of the stabilization parameter γ_0.

The element-wise relative errors in L^2 norm for the displacement field are plotted in Figure (13) for specific choices of the meshes: for conforming IGA we use a 8×8 mesh as before, whereas for Nitsche's

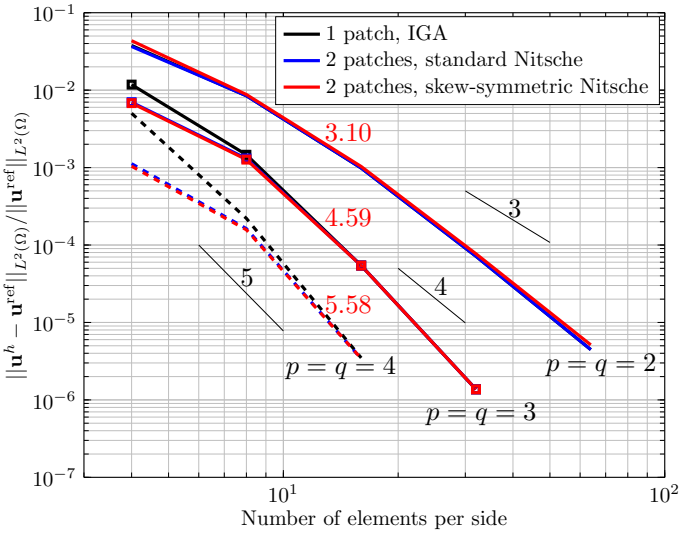

(a) L^2 norm

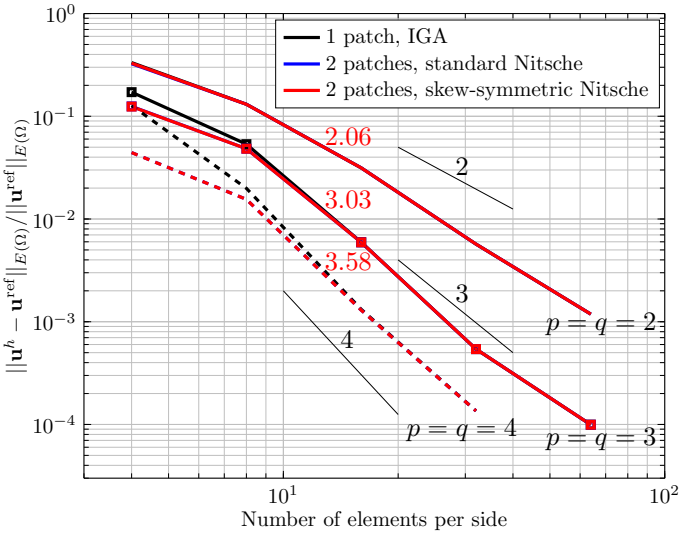

(b) Energy norm

Figure 12: Patch coupling of two plates: relative errors of displacement field in L^2 norm (a) and energy norm (b).

Table 2: Patch coupling of two plates: condition numbers ($\times 10^{10}$) of the obtained stiffness matrix. The standard Nitsche's formulation increases the condition number significantly.

Method	Number of elements per side	$p=q=2$	$p=q=3$	$p=q=4$	$p=q=5$
Conforming IGA	4	0.926	0.884	0.858	0.850
	8	0.958	0.979	1.103	1.238
	16	0.959	1.002	1.161	1.347
Standard Nitsche	4	8.942	15.033	21.711	28.011
	8	11.963	18.104	23.693	29.033
	16	13.301	21.680	29.204	35.938
Skew-symmetric Nitsche	4	1.919	1.340	1.285	1.256
	8	2.118	2.055	2.039	2.035
	16	2.174	2.487	2.723	2.887

formulations a 4×8 mesh in the left patch and a 5×5 mesh in the right patch. Generally the errors due to Nitsche's patch coupling, though acceptable, are larger than conforming IGA, and the results of the standard and skew-symmetric Nitsche's coupling are comparable.

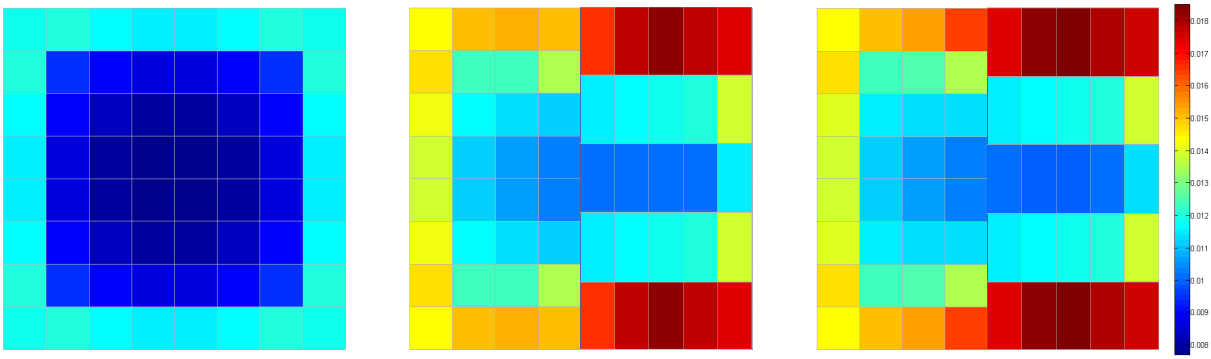

(a) Conforming IGA (b) Standard Nitsche's coupling (c) Skew-symmetric Nitsche's coupling

Figure 13: Patch coupling of two plates: element-wise relative errors of displacement field in L^2 norm $||\mathbf{u}^h - \mathbf{u}^{\text{ref}}||_{L^2(\Omega^e)}/||\mathbf{u}^{\text{ref}}||_{L^2(\Omega^e)}$. For conforming IGA the mesh is 8×8, for two patch coupling the meshes are 4×8 and 5×5.

4.2.2. Patch coupling of an annular plate

In this subsection we show that for several curved interfaces that needed to be glued, Nitsche's formulation is accurate regarding the smoothness and errors of the coupled physical field. Figure (14) shows an annular plate subjected to a uniformly distributed load f, with thickness $t = 10^{-1}$, Young's modulus $E = 200 \times 10^9$ and Poisson's ratio $\nu = 0.3$, The outer edge of the plate is fixed and inner edge is free. The model is divided into 8 patches with different meshes, then it leads to 4 curved interfaces and 8 straight interfaces as shown in Figure (15), thus this problem still corresponds to setting described in 3.4. We make use of an IGA approximation with bi-quadratic degenerated Reissner-Mindlin elements [1]. The stabilization parameter γ_0

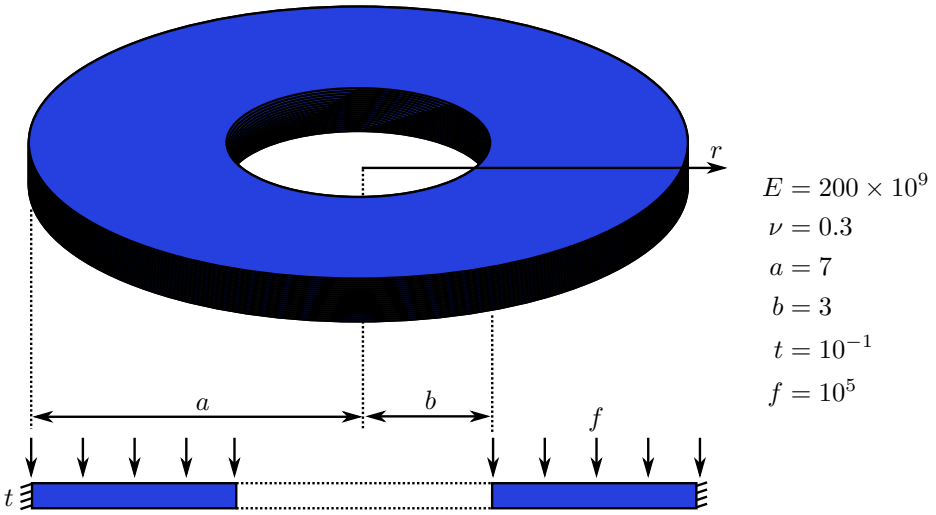

Figure 14: An annular plate under uniformly distributed load f, the outer edge is fixed.

is still computed by solving the generalized eigenvalue problem (9). The analytical solution for the transverse deflection can be found in [89], and the largest deflection is $w^{\text{ref}}_{r=b} = -0.10409$.

The results obtained with standard and the skew-symmetric Nitsche's formulations are plotted in Figure (16) and Figure (17), respectively. Although the model is discretized with different meshes, the deflection field is quite smooth, implying that Nitsche's method is effective to glue curved patches with non-conforming meshes. Visible errors are noticed at patch 0 and patch 4, which makes sense because the mesh for patch 0 is relatively coarse. The errors of the largest deflection for the skew-symmetric and the standard Nitsche's formulations are -0.58% and -0.12%, respectively.

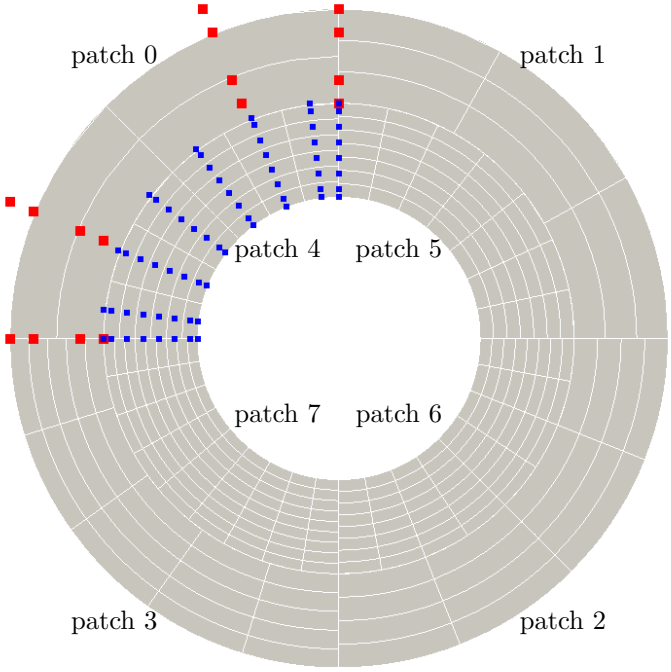

Patch no.	Mesh $\xi \times \eta$	Control points
0	2×2	4×4
1	3×3	5×5
2	4×4	6×6
3	5×5	7×7
4	6×6	8×8
5	7×7	9×9
6	8×8	10×10
7	9×9	11×11

Figure 15: The annular plate is divided into 8 non-matching patches with 4 curved interfaces and 8 straight interfaces.

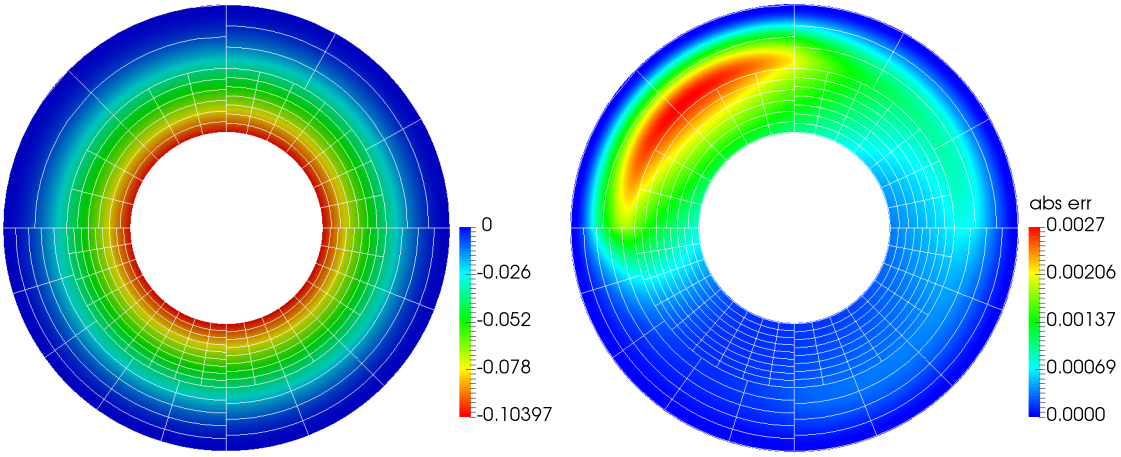

(a) Deflection field $\mathbf{u}^h$

(b) Absolute error $|\mathbf{u}^h - \mathbf{u}^{\text{ref}}|$

Figure 16: Results of the annular plate, using standard Nitsche's formulation and the mesh given in Figure (15).

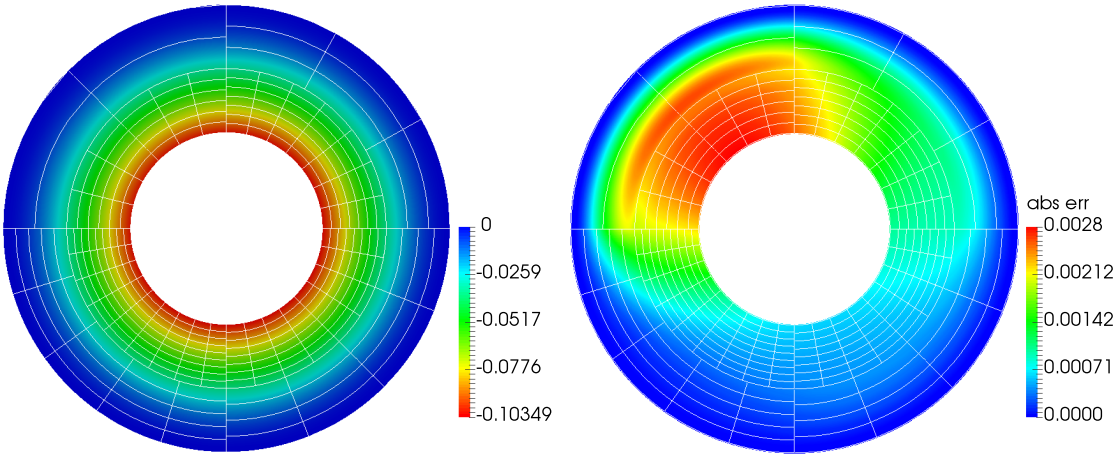

(a) Deflection field $\mathbf{u}^h$ (b) Absolute error $|\mathbf{u}^h - \mathbf{u}^{\text{ref}}|$

Figure 17: Results of the annular plate, using skew-symmetric Nitsche's formulation and the mesh given in Figure (15).

4.2.3. Patch coupling effects: modal analysis

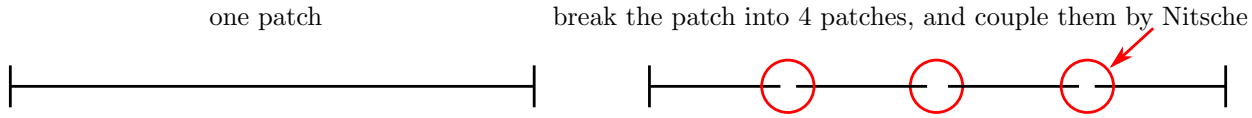

Figure 18: Rod model. On the left, one patch rod model is adopted for comparison. On the right, the rod is artificially broken into four patches and the additional three interfaces are coupled by Nitsche's method.

To study whether additional effects are introduced in modal analysis by Nitsche's coupling, the longitudinal vibration of a rod [30] is considered in Figure (18). On the right side of the figure, the rod model is broken into four identical patches and they are coupled by Nitsche's method. We adapt the framework presented in 3.4 to this simpler model and to a vibration setting. So we find $u : (0,1) \to \mathbb{R}$ and $\omega^2 > 0$ that solve:

$$u_{,xx} + \omega^2 u = 0, \text{ on } (0,1),$$
$$u(0) = u(1) = 0,$$

and we know the exact natural frequencies are

$$\omega_n = n\pi, \quad n = 1, \ldots, N,$$

with N being the total number of DoFs.

The discrete spectra is normalized by N, and the normalized discrete spectra is given in Figure (19),

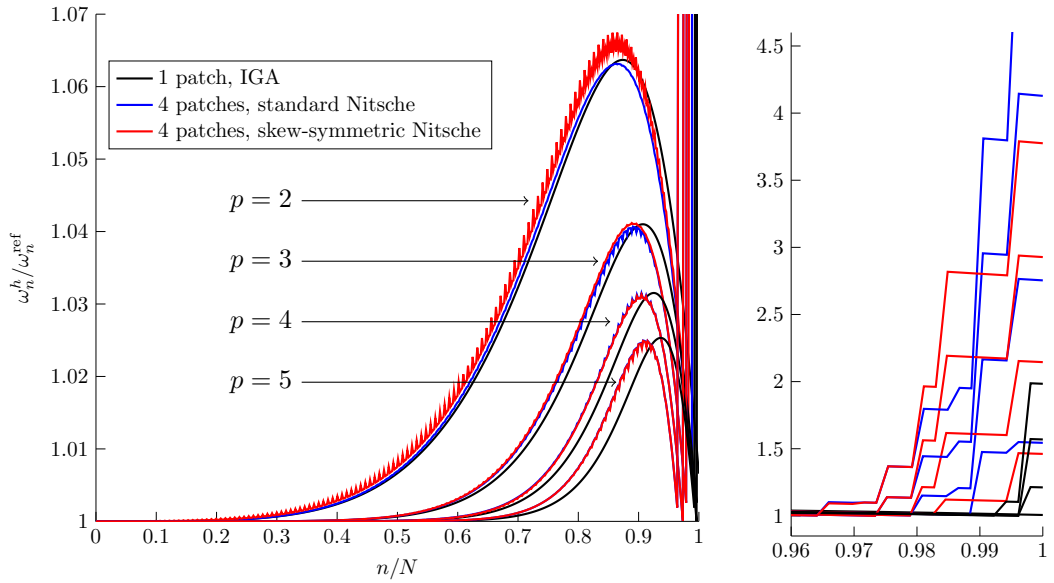

Figure 19: Normalized discrete spectra. As shown in the right figure, the sudden jump of the frequencies identify the "outliers". More details are shown in Figure (20).

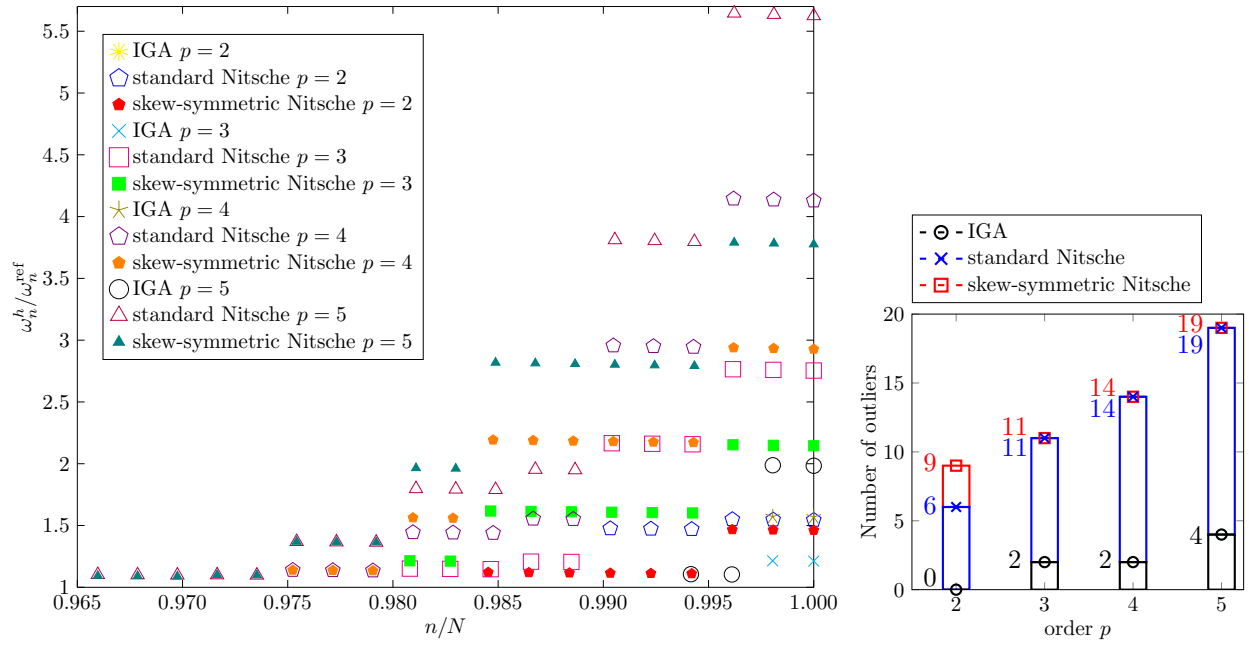

Figure 20: Normalized outlier frequencies. The model coupled by Nitsche's leads to a larger number of "outliers". The corresponding outlier eigenmodes of $p = 2$ are plotted in Figure (21) for the standard Nitsche's formulation and in Figure (22) for the skew-symmetric Nitsche's formulation.

showing that Nitsche's coupled model is almost as accurate as conforming IGA for lower frequencies, specifically $n/N < 0.2$ for $p = 2$ and $n/N < 0.5$ for $p > 2$. For higher frequencies, the skew-symmetric Nitsche's formulation leads to oscillations when $p = 2$, and the solutions from both standard and skew-symmetric Nitsche's formulations are oscillatory when $p = 3, 4, 5$.

At the very end of the spectra, the sudden jumps of the frequencies are known as the "outliers" [30, 21, 48], as shown in the enlarged figure on the right side of Figure (19). These "outlier" frequencies are drawn in Figure (20), and the number of outliers is also counted. The "outlier" frequencies are captured near $n/N = 1$ by the conforming IGA, and the model coupled by Nitsche's formulation leads to a larger number of "outliers". The corresponding outlier eigenmodes of $p = 2$ are plotted in Figure (21) for the standard Nitsche's formulation and in Figure (22) for the skew-symmetric Nitsche's formulation. To achieve a better demonstration of the eigenmodes, we plot the longitudinal deformation along the vertical axis. For the skew-symmetric formulation, there exist 3 pairs of symmetrical eigenmodes, i.e. no. 510 and no. 511, no. 512 and no. 513, no. 514 and no. 515. These results imply that the action of coupling the interfaces by Nitsche's method increases the number of "outliers", and the eigenmodes correspond to these "outliers" are highly localized at these coupled interfaces.

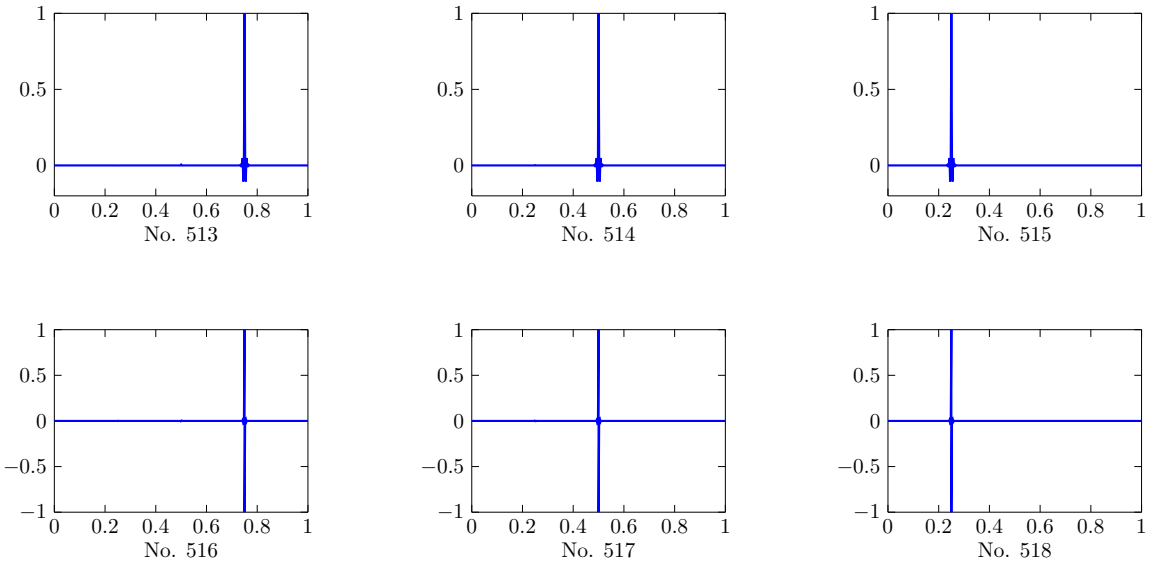

Figure 21: "Outlier" (last 6 out of 518) eigenmodes obtained by the standard Nitsche's formulation with $p = 2$. The longitudinal deformations are plotted along the vertical axis. The eigenmodes that correspond to the "outlier" are highly localized at the coupled interfaces.

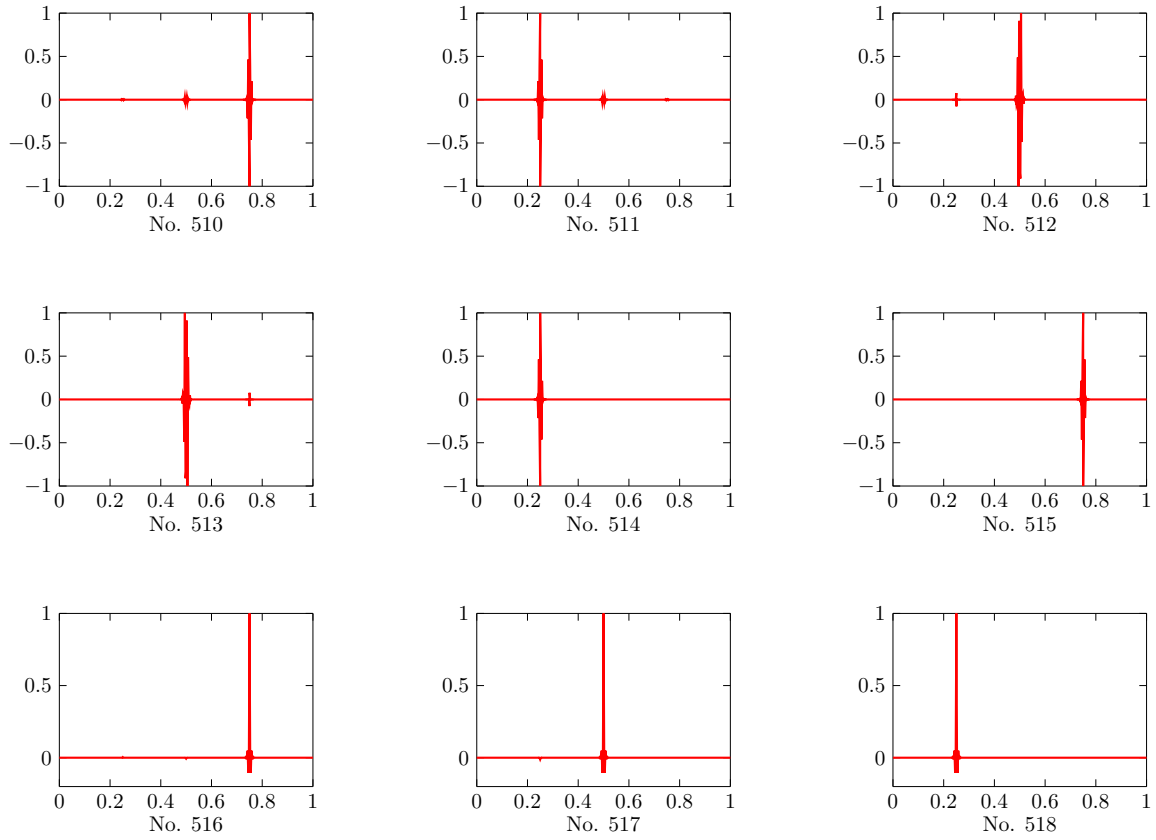

Figure 22: "Outlier" (last 9 out of 518) eigenmodes obtained by the skew-symmetric Nitsche's formulation with $p = 2$. The longitudinal deformations are plotted along the vertical axis. The eigenmodes that correspond to the "outlier" are highly localized at the coupled interfaces.

4.3. Frictionless contact

In the following examples only NURBS basis functions of order $p = q = 2$ are employed, since this approximation order is sufficient for the wide majority of contact problems (see Remark 4). Note that for contact problems the skew-symmetric Nitsche's formulation can not be parameter-free anymore (see Remark 2).

4.3.1. Hertz contact

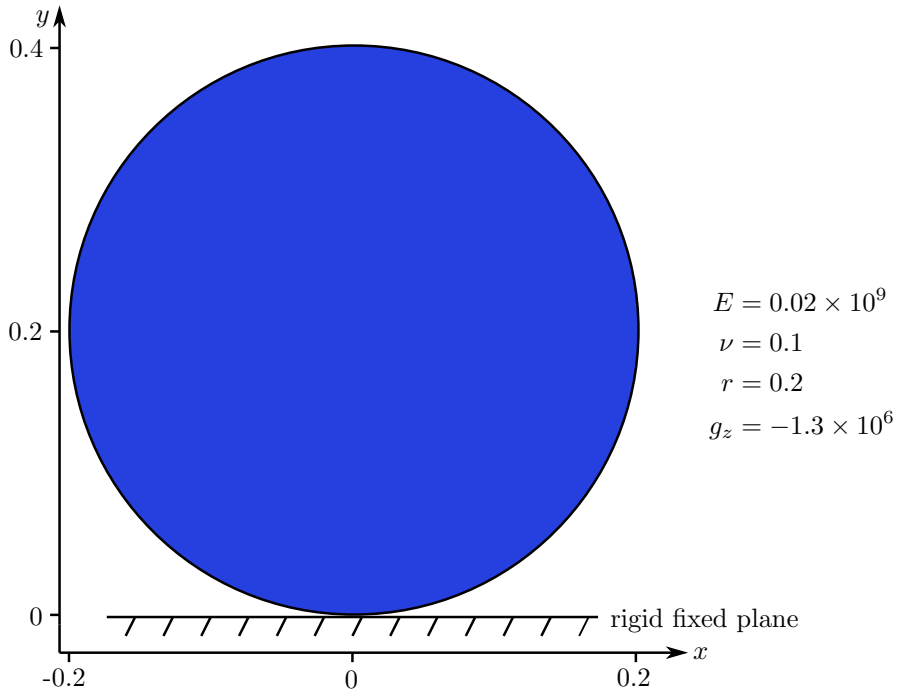

Figure 23: Hertz contact example, the contact between a linear elastic disc under a vertical gravity force and a rigid fixed plane. Values for the Young modulus E, Poisson ratio ν, radius r and gravity load g_z are provided.

In this section we show that the proposed contact formulation described in Section 3.5 is able to predict the contact pressure distribution versus contact width to some degree of accuracy, and the skew-symmetric formulation is robust w.r.t. the choice of the stabilization parameter γ_0. The Hertz contact assumes an elastic frictionless contact without adhesive forces between two cylinders with the same height, radii and elasticity moduli. To simplify, one cylinder (master body) is fixed, its material is set to be rigid, and its contact surface is flat. More precisely we study a contact problem as shown in Figure (23), which analytical solution was provided by Hertz [90]. Thus we consider the setting 3.5.1 and a Signorini-type problem (with a rigid support). The boundary conditions are the following: the bottom of the disc is specified as the

potential contact boundary, and the whole disc is subjected to a vertical gravity force g_z. To prevent rigid body motions we fix the horizontal displacement at several control points along axis $x = 0$.

To begin with we draw the results for one case in Figure (24) as an illustration, using the skew-symmetric Nitsche's contact formulation with 8×8 elements. The displacement magnitude field shows that the rigid fixed plane has successfully prevented the disc from dropping down, and the contact surface of the elastic disc adjusts itself to match the rigid fixed plane, resulting in a straight contact surface.

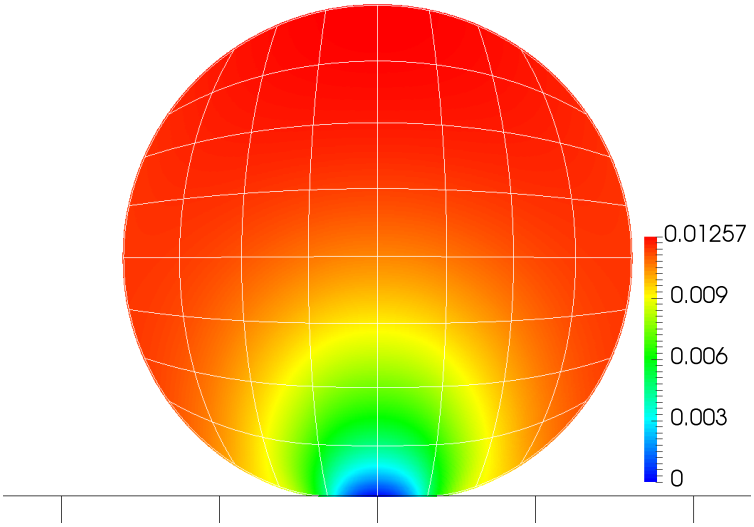

Figure 24: Contour plot of displacement magnitude field obtained by the skew-symmetric Nitsche's method with 8×8 elements.

The pressure distribution with respect to the contact width is plotted and compared with the analytical solution in Figure (25), according to the fact that the stress on the contact surface reaches balance with the contact pressure. Both standard and skew-symmetric contact formulations are employed. The contact stresses in blue and red dots are calculated at quadrature points. Nitsche's method can properly predict the pressure distribution with respect to the contact width as the mesh is refined.

Table 3: Hertz contact: number of semi-smooth Newton iterations for various γ_0.

Method	$\gamma_0 =$	Mesh 4×4	Mesh 8×8	Mesh 16×16	Mesh 32×32	Mesh 64×64
Standard	γ_0^{ref}	8	13	21	41	52
Nitsche	$\gamma_0^{\text{ref}}/10000$	6	9	11	> 100	> 100
	$\gamma_0^{\text{ref}}/100000$	7	22	9	52	45
Skew-symmetric	γ_0^{ref}	8	13	21	42	52
Nitsche	$\gamma_0^{\text{ref}}/10000$	6	7	10	9	11
	$\gamma_0^{\text{ref}}/100000$	7	7	9	9	10

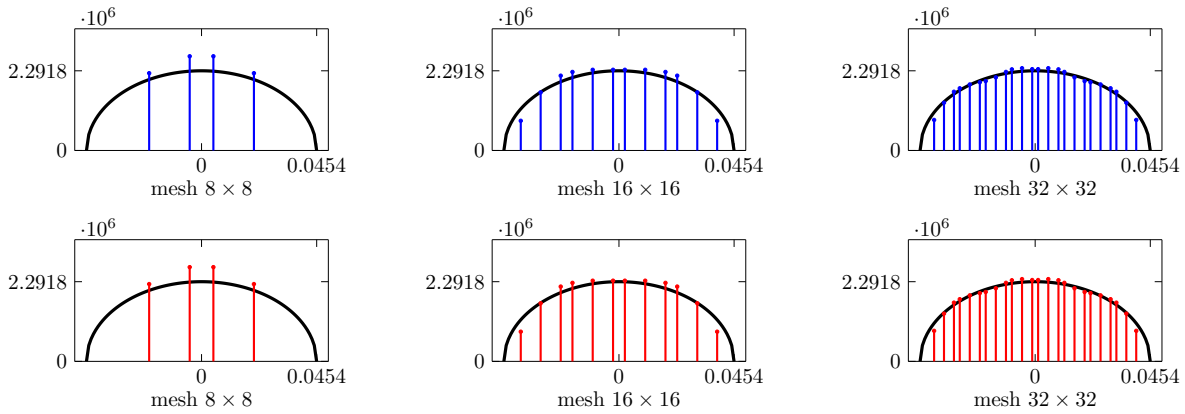

Figure 25: Pressure distribution for Hertz contact. Horizontal axis: contact surface. Vertical axis: contact pressure p. — analytical solution, — the standard Nitsche's method, — the skew-symmetric Nitsche's method. The contact stresses are calculated at quadrature points.

The number of semi-smooth Newton iterations for various values of the stabilization parameter γ_0 are displayed in Table (3). We define $\gamma_0^{\text{ref}} := 2\lambda^{h,\text{MAX}}$, and then study the influence of γ_0 by choosing $\gamma_0 = \gamma_0^{\text{ref}}$, $\gamma_0 = \gamma_0^{\text{ref}}/10000$, and $\gamma_0 = \gamma_0^{\text{ref}}/100000$. For $\gamma_0 = \gamma_0^{\text{ref}}$ the standard Nitsche's formulation and the skew-symmetric one behave similarly, and the number of iterations increases as the mesh is refined, since the problem becomes stiffer. For $\gamma_0 = \gamma_0^{\text{ref}}/10000$ and $\gamma_0 = \gamma_0^{\text{ref}}/100000$ the skew-symmetric formulation remains remarkably robust and converges faster than for $\gamma_0 = \gamma_0^{\text{ref}}$. Conversely, convergence is harder to achieve with the standard formulation, especially for finer meshes, because these small values of γ_0 can not ensure well-posedness anymore. These results are coherent with the behavior observed for FEM in [61].

The convergence performance is studied, compared to a reference solution using 128×128 elements. For γ_0^{ref}, the convergence curves for standard and skew-symmetric Nitsche's formulations are similar and we recover a rate of 1.41, close to what is expected for such a problem and a discretization of order 2 (see Remark 4 and [27]). For $\gamma_0^{\text{ref}}/100000$, as displayed in Figure (26), the convergence curves for standard Nitsche's method are perturbed and the convergence rate is lower. This is in agreement with the theory that standard Nitsche's formulation requires γ_0 large enough to ensure well-posedness and optimal convergence, see 3.2. Conversely, the convergence performance for skew-symmetric Nitsche's method is not affected by the choice of γ_0. All this is in agreement with the theory and previous observations for FEM discretization, see, e.g., [27].

4.3.2. Contact between two blocks

The goal of this section is to test whether the proposed formulation can properly impose the contact conditions through non-matching elements, and preliminarily investigate the performance of both biased and

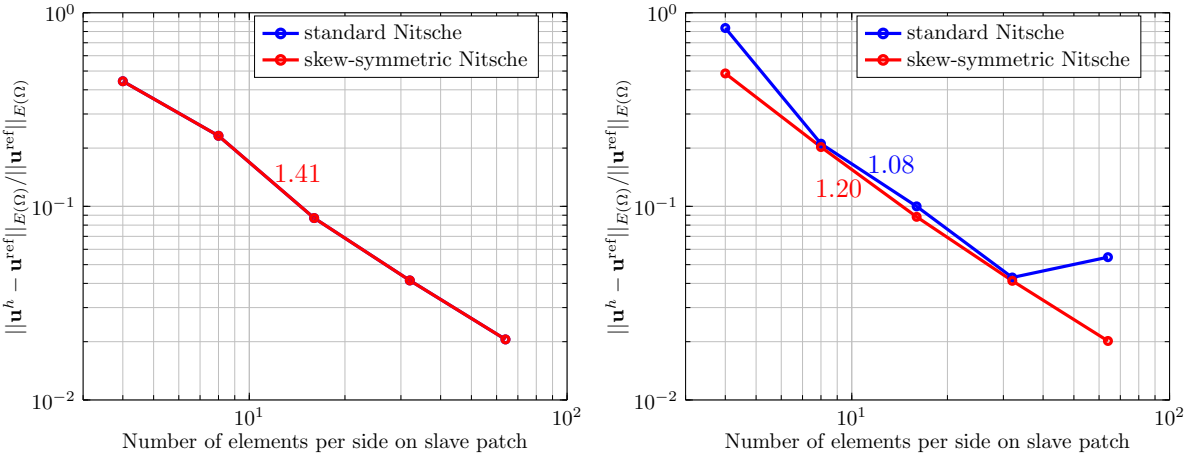

(a) $\gamma_0 = \gamma_0^{\text{ref}}$ (b) $\gamma_0 = \gamma_0^{\text{ref}}/100000$

Figure 26: Hertz contact: relative errors of displacement field in energy norm.

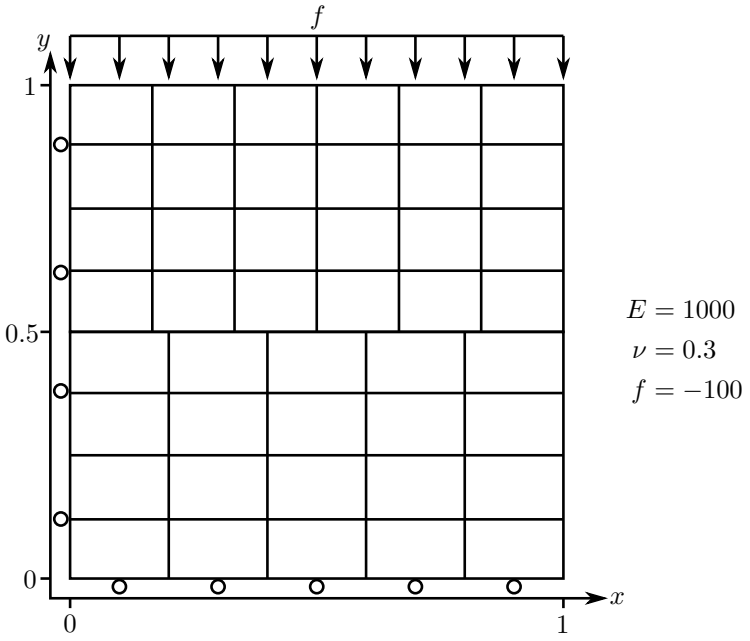

Figure 27: Two blocks with non-matching meshes. The upper block is subjected to a uniform pressure load f on its top. Both blocks have the same material properties. On the left and at the bottom of the structure, we impose a sliding condition, while on the right we impose no traction. Remark that the problem setup is not symmetric.

unbiased variants of the standard and skew-symmetric contact formulations. The corresponding framework is described in 3.5.1. The classical contact patch test proposed by Taylor [80] is used to examine the contact algorithm and investigate whether it transfers the constant contact pressure through the contact surface even for non-matching meshes [32]. In order to enforce a uniform pressure on the top surface easily, we adopt a modified patch test [31, 39] as shown in Figure (27), where the material properties and the boundary conditions are provided. The resulting test setup is similar as in [85]. Because of the boundary conditions along both sides of the two blocks, this problem setup is not symmetric. The reference solution of this (plane stress) problem is given by

$$\begin{aligned} u_x(x,y) &= 0.03x, \quad u_y(x,y) = -0.1y, \\ \sigma_{xx}(x,y) &= 0,\ \sigma_{yy}(x,y) = -100,\ \sigma_{xy}(x,y) = 0, \end{aligned} \tag{24}$$

where u_x and u_y are the components of the displacement $\mathbf{u}$ and where σ_{xx}, σ_{xy} and σ_{yy} are the components of $\boldsymbol{\sigma}(\mathbf{u})$.

We use and compare both the biased Nitsche's contact formulation, which corresponds to subsection 3.5.1, and the unbiased one, which corresponds to subsection 3.5.2. Bi-quadratic basis functions are employed, and only $\gamma_0 = 2\lambda^{h,\mathrm{MAX}}$ is used. Figure (28) and Figure (29) demonstrate the distribution of the relative errors for biased and unbiased skew-symmetric formulation, respectively. For the biased formulation visible errors appear on the slave patch (the upper patch), while for the unbiased formulation they appear on both patches. We list the relative errors for u_y and σ_{yy} in Table (4), showing that for both biased and unbiased versions the accuracy is comparable, which supports the conclusion in [61].

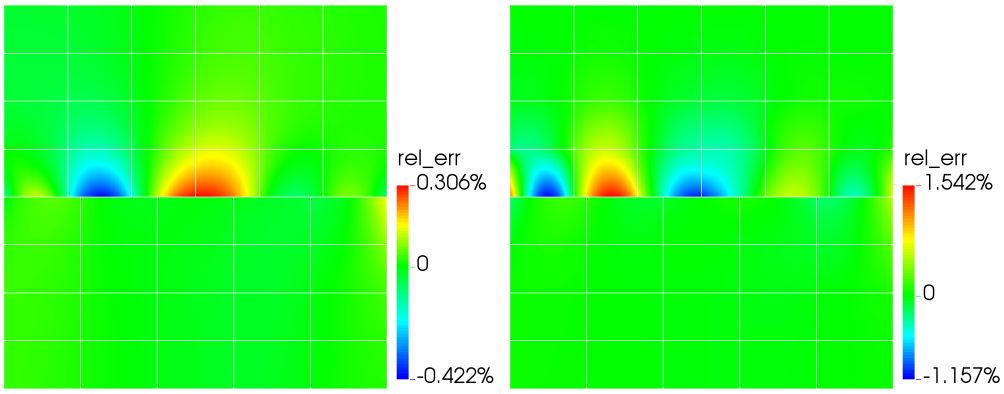

(a) Relative error for u_y (b) Relative error for σ_{yy}

Figure 28: Contact between two blocks: relative errors for the displacement field u_y and for the stress field σ_{yy}. The biased skew-symmetric Nitsche's method is employed with the mesh given in Figure (27).

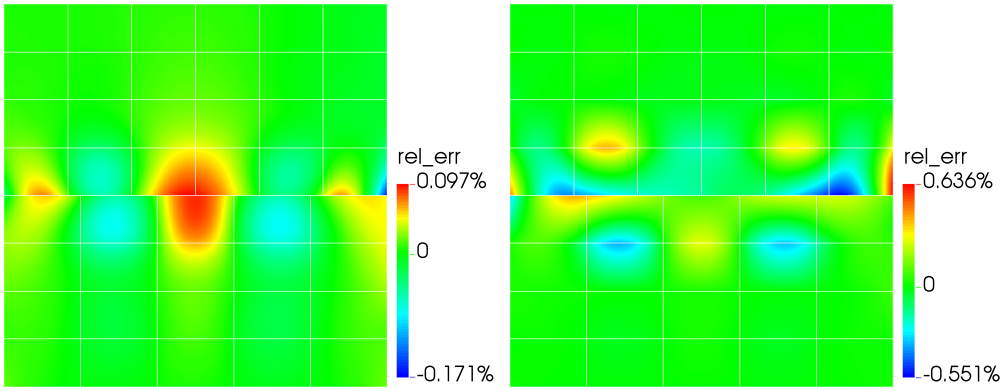

(a) Relative error for u_y (b) Relative error for σ_{yy}

Figure 29: Contact between two blocks: relative errors for the displacement field u_y and for the stress field σ_{yy}. The unbiased skew-symmetric Nitsche's method is employed with the mesh given in Figure (27).

Table 4: Contact between two blocks: ranges of relative errors for u_y and σ_{yy}.

Formulation type	Nitsche's formulation type	Relative errors for u_y	Relative errors for σ_{yy}
Biased	Standard	-0.416% $\sim$ 0.311%	-1.141% $\sim$ 1.518%
Biased	Skew-symmetric	-0.422% $\sim$ 0.306%	-1.157% $\sim$ 1.542%
Unbiased	Standard	-0.279% $\sim$ 0.384%	-2.816% $\sim$ 3.083%
Unbiased	Skew-symmetric	-0.171% $\sim$ 0.097%	-0.551% $\sim$ 0.636%

4.3.3. Self-contact of a 3D clip

Here we present a clip model to illustrate the skew-symmetric Nitsche's formulation for self-contact in 3D, see 3.5.2. The model in shown in Figure (30). It is subjected to a uniform surface traction f on its end. The surface colored in red is defined as the potential contact surface, the gap between the contact surface is $g = 0.01$. The control mesh in 3D is also shown below, from which it is noticed that the contact surface is actually the top-surface itself, thus this is a top-surface to top-surface self-contact problem. Once again we adopt quadratic NURBS basis functions for the model and for the displacement field as well, and use 3 quadrature points for each element boundary along the contact surface. The value of $\gamma_0 = 2\lambda^{h,\mathrm{MAX}}$ comes from the generalized eigenvalue problem (Eq. (9)).

The contour plot of the vertical displacement field u_z is shown in Figure (31). When the iterative solving starts, the contact surface is penetrated, the largest vertical displacement is $u_z = -0.09413$ while the contact gap is $g = 0.01$, see Figure (31) (a) (this is what the deformation would be if no contact were taken into account). When semi-smooth Newton procedure has converged, the largest vertical displacement becomes $u_z = -0.01024$, see Figure (31) (b). In Figure (31) (c) we adopt the results obtained by *ABAQUS* using a sufficient number of 3D solid elements: the vertical displacement distribution obtained by Nitsche's

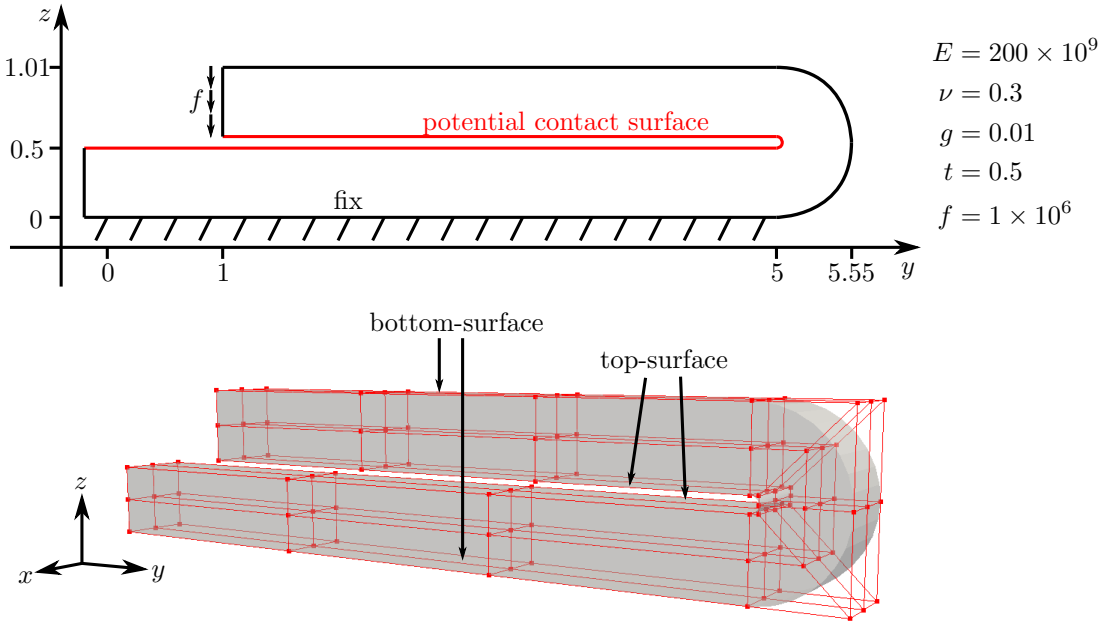

Figure 30: A 3D clip model with thickness t and a small gap g. Its initial control points and control net are also shown. The values of the physical parameters are provided.

contact formulation is in good agreement with the solution provided by *ABAQUS*. The relative errors of the maximum positive and negative vertical displacements are 0.196% and −3.042% respectively.

5. Conclusions

We presented a systematic way to derive Nitsche's formulations for different kind of boundary and interface conditions, and studied this technique in the context of isogeometric analysis (IGA) discretization. We recover different variants of Nitsche's method, for different values of the *Nitsche parameter* θ, and then focused on the skew-symmetric variant, namely $\theta = -1$. This variant is appealing because it does not need a stabilization term for linear boundary/interface conditions, and is robust w.r.t. the stabilization parameter for non-linear boundary/interface conditions. Several numerical studies were performed to illustrate the behavior of Nitsche's method, especially the skew-symmetric variant. From the numerical results we can state the observations below:

- The skew-symmetric formulation is effective to impose Dirichlet displacement boundary conditions in small strain elasticity as well as the symmetric rotational boundary conditions for Kirchhoff-Love plates. The skew-symmetric formulation is parameter-free in this context and achieves good accuracy: for the circular patch test (Figure (7)) and the Kirchhoff plate (Figure (10)) we observe the predicted optimal convergence rates in the energy norm.

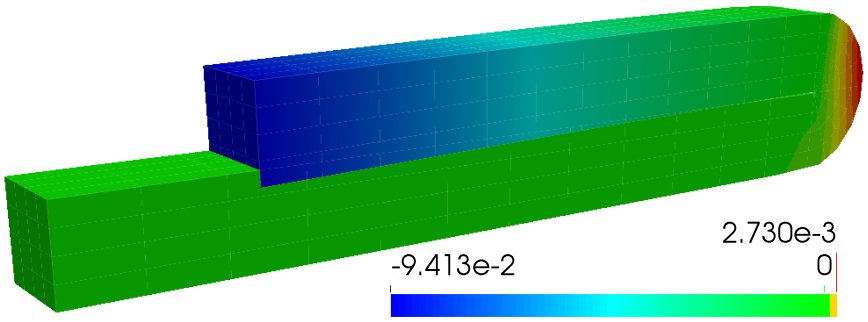

(a) Skew-symmetric Nitsche's self-contact formulation: 1st iteration

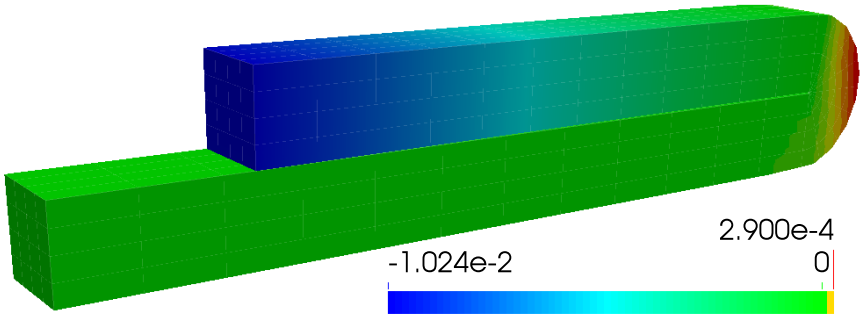

(b) Skew-symmetric Nitsche's self-contact formulation: converged solution

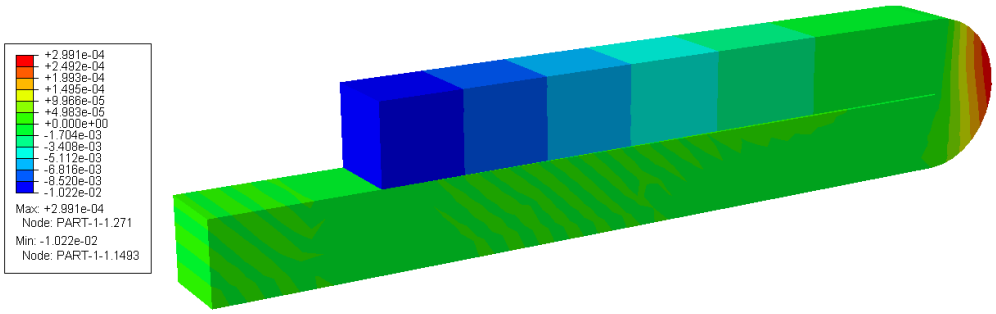

(c) *ABAQUS* reference solution. $u_z^{\mathrm{MAX}} = 2.991 \times 10^{-4}$, $u_z^{\mathrm{MIN}} = -1.022 \times 10^{-2}$.

Figure 31: Contour plot of vertical displacement field u_z.

• For patch coupling in statics, the skew-symmetric Nitsche's formulation is still parameter-free. Condition numbers for the global stiffness matrix are far better than for standard Nitsche, and only slightly above the conforming setting. They are also almost independent of the mesh size, and basis functions orders: see Table (2) in Section 4.2.1.

• For patch coupling in modal analysis, Nitsche's formulation increases the number of "outlier" frequencies. The reason is believed to be that Nitsche's formulation introduces additional highly localized eigenmodes, and the positions of these newly added eigenmodes just locate at the coupled interfaces.

• For contact problems in linear elasticity, the skew-symmetric Nitsche's formulation behaves more robustly than the standard Nische formulation regarding the value of the stabilization parameter. Nitsche's method can properly impose the contact conditions, and predict the pressure distribution with respect to the contact width. Moreover, it allows an unbiased variant that can be more appealing for self-body and multi-body contact.

Acknowledgments

The authors thank the two anonymous referees for their constructive comments that helped to improve the paper. They thank also Patrick Le Tallec for inspiring discussions and comments that helped to improve the presentation. Qingyuan Hu is funded by China Scholarship Council. Stéphane Bordas thanks the financial support of the European Research Council Starting Independent Research Grant (ERC Stg grant agreement No. 279578). Stéphane Bordas is also grateful for the support of the Fonds National de la Recherche Luxembourg FNRS-FNR grant INTER/FNRS/15/11019432/EnLightenIt/Bordas. Franz Chouly thanks Région Bourgogne Franche-Comté for funding ("Convention Région 2015C-4991. Modèles mathématiques et méthodes numériques pour l'élasticité non-linéaire"), as well as the Centre National de la Recherche Scientifique ("Convention 232789 DEFI InFIniTI 2017 - Projet MEFASIM").

References

[1] Adam, C., Bouabdallah, S., Zarroug, M., and Maitournam, H. Improved numerical integration for locking treatment in isogeometric structural elements. part II: Plates and shells. *Computer Methods in Applied Mechanics and Engineering 284* (2015), 106–137.

[2] Annavarapu, C., Hautefeuille, M., and Dolbow, J. E. A robust Nitsches formulation for interface problems. *Computer Methods in Applied Mechanics and Engineering 225* (2012), 44–54.

[3] Antolin, P., Buffa, A., and Fabre, M. A priori error for unilateral contact problems with lagrange multiplier and isogeometric analysis. *arXiv preprint arXiv:1701.03150* (2017).

[4] Apostolatos, A., Schmidt, R., Wüchner, R., and Bletzinger, K.-U. A Nitsche-type formulation and comparison of the most common domain decomposition methods in isogeometric analysis. *International Journal for Numerical Methods in Engineering 97*, 7 (2014), 473–504.

[5] Auliac, S., Belhachmi, Z., Ben Belgacem, F., and Hecht, F. Quadratic finite elements with non-matching grids for the unilateral boundary contact. *ESAIM Math. Model. Numer. Anal. 47*, 4 (2013), 1185–1203.

[6] Babuška, I. The finite element method with Lagrangian multipliers. *Numerische Mathematik 20* (1972/73), 179–192.

[7] Babuška, I. The finite element method with penalty. *Mathematics of Computation 27*, 122 (1973), 221–228.

[8] Bazilevs, Y., Beirao da Veiga, L., Cottrell, J. A., Hughes, T. J., and Sangalli, G. Isogeometric analysis: approximation, stability and error estimates for h-refined meshes. *Mathematical Models and Methods in Applied Sciences 16*, 07 (2006), 1031–1090.

[9] Becker, R., Hansbo, P., and Stenberg, R. A finite element method for domain decomposition with non-matching grids. *ESAIM: Mathematical Modelling and Numerical Analysis 37*, 2 (2003), 209–225.

[10] Beer, G., Marussig, B., and Duenser, C. Isogeometric boundary element method for the simulation of underground excavations. *Geotechnique letters 3*, 3 (2013), 108–111.

[11] Beirão da Veiga, L., Buffa, A., Sangalli, G., and Vázquez, R. Mathematical analysis of variational isogeometric methods. *Acta Numerica 23* (2014), 157–287.

[12] Ben Belgacem, F. The mortar finite element method with Lagrange multipliers. *Numerische Mathematik 84*, 2 (1999), 173–197.

[13] Benson, D., Bazilevs, Y., Hsu, M.-C., and Hughes, T. Isogeometric shell analysis: the Reissner–Mindlin shell. *Computer Methods in Applied Mechanics and Engineering 199*, 5 (2010), 276–289.

[14] Benson, D., Bazilevs, Y., Hsu, M.-C., and Hughes, T. A large deformation, rotation-free, isogeometric shell. *Computer Methods in Applied Mechanics and Engineering 200*, 13 (2011), 1367–1378.

[15] Bernardi, C., Maday, Y., and Patera, A. T. Domain decomposition by the mortar element method. In *Asymptotic and numerical methods for partial differential equations with critical parameters (Beaune, 1992)*, vol. 384 of *NATO Adv. Sci. Inst. Ser. C Math. Phys. Sci.* Kluwer Acad. Publ., Dordrecht, 1993, pp. 269–286.

[16] Bernardi, C., Maday, Y., and Patera, A. T. A new nonconforming approach to domain decomposition: the mortar element method. In *Nonlinear partial differential equations and their applications. Collège de France Seminar, Vol. XI (Paris, 1989–1991)*, vol. 299 of *Pitman Res. Notes Math. Ser.* Longman Sci. Tech., Harlow, 1994, pp. 13–51.

[17] Boiveau, T., and Burman, E. A penalty-free Nitsche method for the weak imposition of boundary conditions in compressible and incompressible elasticity. *IMA Journal of Numerical Analysis 36*, 2 (2016), 770–795.

[18] Brivadis, E., Buffa, A., Wohlmuth, B., and Wunderlich, L. Isogeometric mortar methods. *Computer Methods in Applied Mechanics and Engineering 284* (2015), 292–319.

[19] Burman, E. A penalty-free nonsymmetric Nitsche-type method for the weak imposition of boundary conditions. *SIAM Journal on Numerical Analysis 50*, 4 (2012), 1959–1981.

[20] Burman, E., Hansbo, P., and Larson, M. G. The penalty free Nitsche method and nonconforming finite elements for the Signorini problem. *SIAM Journal on Numerical Analysis 55*, 6 (2017), 2523–2539.

[21] Cazzani, A., Stochino, F., and Turco, E. An analytical assessment of finite element and isogeometric analyses of the whole spectrum of timoshenko beams. *ZAMM-Journal of Applied Mathematics and Mechanics/Zeitschrift für Angewandte Mathematik und Mechanik 96*, 10 (2016), 1220–1244.

[22] Chen, J., Li, C., and Chen, W. A family of spline finite elements. *Computers & Structures 88*, 11 (2010), 718–727.

[23] Chouly, F. An adaptation of Nitsche's method to the tresca friction problem. *Journal of Mathematical Analysis and Applications 411*, 1 (2014), 329–339.

[24] Chouly, F., Fabre, M., Hild, P., Mlika, R., Pousin, J., and Renard, Y. An overview of recent results on Nitsche's method for contact problems. *Lecture Notes in Computational Science and Engineering 121* (2017), 93–141. Proceedings of the UCL Workshop 2016 on Geometrically Unfitted Finite Element Methods and Applications. Editors: Stéphane Bordas, Erik Burman, Mats G. Larson and Maxim Olshanskii.

[25] Chouly, F., and Hild, P. A Nitsche-based method for unilateral contact problems: numerical analysis. *SIAM Journal on Numerical Analysis 51*, 2 (2013), 1295–1307.

[26] Chouly, F., Hild, P., Lleras, V., and Renard, Y. Nitsche-based finite element method for contact with Coulomb friction. *Lecture Notes in Computational Science and Engineering*. To appear. Proceedings of the European Conference on Numerical Mathematics and Advanced Applications ENUMATH 2017. Editor: Jan Martin Nordbotten.

[27] Chouly, F., Hild, P., and Renard, Y. Symmetric and non-symmetric variants of Nitsche's method for contact problems in elasticity: theory and numerical experiments. *Mathematics of Computation 84*, 293 (2015), 1089–1112.

[28] Chouly, F., Mlika, R., and Renard, Y. An unbiased Nitsche's approximation of the frictional contact between two elastic structures. *Numerische Mathematik* (2018). To appear. `https://doi.org/10.1007/s00211-018-0950-x`.

[29] Cottrell, J. A., Hughes, T. J., and Bazilevs, Y. *Isogeometric analysis: toward integration of CAD and FEA*. John Wiley & Sons, 2009.

[30] Cottrell, J. A., Reali, A., Bazilevs, Y., and Hughes, T. J. Isogeometric analysis of structural vibrations. *Computer Methods in Applied Mechanics and Engineering 195*, 41 (2006), 5257–5296.

[31] Crisfield, M. Re-visiting the contact patch test. *International Journal for Numerical Methods in Engineering 48*, 3 (2000), 435–449.

[32] De Lorenzis, L., Evans, J., Hughes, T., and Reali, A. Isogeometric collocation: Neumann boundary conditions and contact. *Computer Methods in Applied Mechanics and Engineering 284* (2015), 21–54.

[33] De Lorenzis, L., Wriggers, P., and Zavarise, G. A mortar formulation for 3D large deformation contact using nurbs-based isogeometric analysis and the augmented lagrangian method. *Computational Mechanics 49*, 1 (2012), 1–20.

[34] Dimitri, R., De Lorenzis, L., Scott, M., Wriggers, P., Taylor, R., and Zavarise, G. Isogeometric large deformation frictionless contact using t-splines. *Computer Methods in Applied Mechanics and Engineering 269* (2014), 394–414.

[35] Dörsek, P., and Melenk, J. M. Adaptive *hp*-FEM for the contact problem with Tresca friction in linear elasticity: the primal-dual formulation and a posteriori error estimation. *Appl. Numer. Math. 60*, 7 (2010), 689–704.

[36] Du, X., Zhao, G., and Wang, W. Nitsche method for isogeometric analysis of Reissner-Mindlin plate with non-conforming multi-patches. *Computer Aided Geometric Design 35/36* (2015), 121–136.

[37] Dunant, C., Vinh, P. N., Belgasmia, M., Bordas, S., and Guidoum, A. Architecture tradeoffs of integrating a mesh generator to partition of unity enriched object-oriented finite element software. *European Journal of Computational Mechanics/Revue Européenne de Mécanique Numérique 16*, 2 (2007), 237–258.

[38] Echter, R., Oesterle, B., and Bischoff, M. A hierarchic family of isogeometric shell finite elements. *Computer Methods in Applied Mechanics and Engineering 254* (2013), 170–180.

[39] El-Abbasi, N., and Bathe, K.-J. Stability and patch test performance of contact discretizations and a new solution algorithm. *Computers & Structures 79*, 16 (2001), 1473–1486.

[40] Embar, A., Dolbow, J., and Harari, I. Imposing Dirichlet boundary conditions with Nitsche's method and spline-based finite elements. *International Journal for Numerical Methods in Engineering 83*, 7 (2010), 877–898.

[41] Freund, J., and Stenberg, R. On weakly imposed boundary conditions for second order problems. In *Proceedings of the Ninth International Conference on Finite Elements in Fluids* (1995), Venice, pp. 327–336.

[42] Guo, Y., and Ruess, M. Nitsche's method for a coupling of isogeometric thin shells and blended shell structures. *Computer Methods in Applied Mechanics and Engineering 284* (2015), 881–905.

[43] Guo, Y., Ruess, M., and Schillinger, D. A parameter-free variational coupling approach for trimmed isogeometric thin shells. *Computational Mechanics* (2016), 1–23.

[44] Hansbo, P. Nitsche's method for interface problems in computational mechanics. *GAMM-Mitteilungen 28*, 2 (2005), 183–206.

[45] Hansbo, P., and Larson, M. G. Discontinuous Galerkin methods for incompressible and nearly incompressible elasticity by Nitsche's method. *Comput. Methods Appl. Mech. Engrg. 191*, 17-18 (2002), 1895–1908.

[46] Harari, I., and Dolbow, J. Analysis of an efficient finite element method for embedded interface problems. *Computational Mechanics 46*, 1 (2010), 205–211.

[47] Harari, I., and Shavelzon, E. Embedded kinematic boundary conditions for thin plate bending by Nitsche's approach. *International Journal for Numerical Methods in Engineering 92*, 1 (2012), 99–114.

[48] Horger, T., Reali, A., Wohlmuth, B., and Wunderlich, L. Improved approximation of eigenvalues in isogeometric methods for multi-patch geometries and neumann boundaries. *arXiv preprint arXiv:1701.06353* (2017).

[49] Hu, Q., Xia, Y., Natarajan, S., Zilian, A., Hu, P., and Bordas, S. Isogeometric analysis of thin reissner-mindlin plates and shells: Locking phenomena and generalized local $\bar{B}$ method. *arXiv preprint arXiv:1709.00402* (2017).

[50] Hughes, T. J., Cottrell, J. A., and Bazilevs, Y. Isogeometric analysis: CAD, finite elements, nurbs, exact geometry and mesh refinement. *Computer Methods in Applied Mechanics and Engineering 194*, 39 (2005), 4135–4195.

[51] Jiang, W., Annavarapu, C., Dolbow, J. E., and Harari, I. A robust Nitsche's formulation for interface problems with spline-based finite elements. *International Journal for Numerical Methods in Engineering 104*, 7 (2015), 676–696.

[52] Juettler, B., Langer, U., Mantzaflaris, A., Moore, S., and Zulehner, W. Geometry + simulation modules: Implementing isogeometric analysis. *Proc. Appl. Math. Mech. 14*, 1 (2014), 961–962. Special Issue: 85th Annual Meeting of the Int. Assoc. of Appl. Math. and Mech. (GAMM), Erlangen 2014.

[53] Kiendl, J., Bletzinger, K.-U., Linhard, J., and Wüchner, R. Isogeometric shell analysis with Kirchhoff–Love elements. *Computer Methods in Applied Mechanics and Engineering 198*, 49 (2009), 3902–3914.

[54] Kikuchi, N., and Oden, J. T. *Contact problems in elasticity: a study of variational inequalities and finite element methods*, vol. 8 of *SIAM Studies in Applied Mathematics*. Society for Industrial and Applied Mathematics (SIAM), Philadelphia, PA, 1988.

[55] Kim, J.-Y., and Youn, S.-K. Isogeometric contact analysis using mortar method. *International Journal for Numerical Methods in Engineering 89*, 12 (2012), 1559–1581.

[56] Kollmannsberger, S., Özcan, A., Baiges, J., Ruess, M., Rank, E., and Reali, A. Parameter-free, weak imposition of Dirichlet boundary conditions and coupling of trimmed and non-conforming patches. *International Journal for Numerical Methods in Engineering 101*, 9 (2015), 670–699.

[57] Lee, C.-Y., and Oden, J. T. A posteriori error estimation of *h-p* finite element approximations of frictional contact problems. *Comput. Methods Appl. Mech. Engrg. 113*, 1-2 (1994), 11–45.

[58] Lian, H., Kerfriden, P., and Bordas, S. Implementation of regularized isogeometric boundary element methods for gradient-based shape optimization in two-dimensional linear elasticity. *International Journal for Numerical Methods in Engineering 106*, 12 (2016), 972–1017.

[59] Lian, H., Simpson, R. N., and Bordas, S. Stress analysis without meshing: Isogeometric boundary-element method. *Proceedings of the Institution of Civil Engineers: Engineering and Computational Mechanics 166*, 2 (2013), 88–99.

[60] Marussig, B., Zechner, J., Beer, G., and Fries, T.-P. Fast isogeometric boundary element method based on independent field approximation. *Computer Methods in Applied Mechanics and Engineering 284* (2015), 458–488.

[61] Mlika, R., Renard, Y., and Chouly, F. An unbiased Nitsche's formulation of large deformation frictional contact and self-contact. *Computer Methods in Applied Mechanics and Engineering 325*, Supplement C (2017), 265–288.

[62] Moussaoui, M., and Khodja, K. Régularité des solutions d'un problème mêlé Dirichlet-Signorini dans un domaine polygonal plan. *Comm. Partial Differential Equations 17*, 5-6 (1992), 805–826.

[63] Nguyen, V. P., Anitescu, C., Bordas, S. P., and Rabczuk, T. Isogeometric analysis: an overview and computer implementation aspects. *Mathematics and Computers in Simulation 117* (2015), 89–116.

[64] Nguyen, V. P., Kerfriden, P., Brino, M., Bordas, S. P., and Bonisoli, E. Nitsche's method for two and three dimensional nurbs patch coupling. *Computational Mechanics 53*, 6 (2014), 1163–1182.

[65] Nguyen, V. P., Kerfriden, P., Claus, S., and Bordas, S. Nitsche's method method for mixed dimensional analysis: conforming and non-conforming continuum-beam and continuum-plate coupling. *arXiv preprint arXiv:1308.2910* (2013).

[66] Nguyen, V. P., Rabczuk, T., Bordas, S., and Duflot, M. Meshless methods: a review and computer implementation aspects. *Mathematics and Computers in Simulation 79*, 3 (2008), 763–813.

[67] Nitsche, J. Über ein Variationsprinzip zur Lösung von Dirichlet-Problemen bei Verwendung von Teilräumen, die keinen Randbedingungen unterworfen sind. *Abhandlungen aus dem Mathematischen Seminar der Universität Hamburg 36* (1971), 9–15.

[68] Peng, X., Atroshchenko, E., Kerfriden, P., and Bordas, S. Isogeometric boundary element methods for three dimensional static fracture and fatigue crack growth. *Computer Methods in Applied Mechanics and Engineering 316* (2017), 151–185.

[69] Reddy, J. N. *Theory and analysis of elastic plates and shells*. CRC press, 2006.

[70] Renard, Y. Generalized Newton's methods for the approximation and resolution of frictional contact problems in elasticity. *Comput. Methods Appl. Mech. Engrg. 256* (2013), 38–55.

[71] Ruess, M., Schillinger, D., Özcan, A. I., and Rank, E. Weak coupling for isogeometric analysis of non-matching and trimmed multi-patch geometries. *Computer Methods in Applied Mechanics and Engineering 269* (2014), 46–71.

[72] Sauer, R. A., and De Lorenzis, L. An unbiased computational contact formulation for 3d friction. *International Journal for Numerical Methods in Engineering 101*, 4 (2015), 251–280.

[73] Schillinger, D., Harari, I., Hsu, M.-C., Kamensky, D., Stoter, S. K., Yu, Y., and Zhao, Y. The non-symmetric Nitsche method for the parameter-free imposition of weak boundary and coupling conditions in immersed finite elements. *Computer Methods in Applied Mechanics and Engineering 309* (2016), 625–652.

[74] Scott, M. A., Simpson, R. N., Evans, J. A., Lipton, S., Bordas, S. P., Hughes, T. J., and Sederberg, T. W. Isogeometric boundary element analysis using unstructured T-splines. *Computer Methods in Applied Mechanics and Engineering 254* (2013), 197–221.

[75] Seitz, A., Farah, P., Kremheller, J., Wohlmuth, B. I., Wall, W. A., and Popp, A. Isogeometric dual mortar

methods for computational contact mechanics. *Computer Methods in Applied Mechanics and Engineering 301* (2016), 259–280.

[76] Shahbazi, K. An explicit expression for the penalty parameter of the interior penalty method. *Journal of Computational Physics 205*, 2 (2005), 401–407.

[77] Simpson, R., Bordas, S., Lian, H., and Trevelyan, J. An isogeometric boundary element method for elastostatic analysis: 2d implementation aspects. *Computers & Structures 118* (2013), 2–12.

[78] Simpson, R. N., Bordas, S. P., Trevelyan, J., and Rabczuk, T. A two-dimensional isogeometric boundary element method for elastostatic analysis. *Computer Methods in Applied Mechanics and Engineering 209* (2012), 87–100.

[79] Stenberg, R. On some techniques for approximating boundary conditions in the finite element method. *Journal of Computational and Applied Mathematics 63*, 1-3 (1995), 139–148.

[80] Taylor, R. L., and Papadopoulos, P. On a patch test for contact problems in two dimensions. *Nonlinear Computational Mechanics* (1991), 690–702.

[81] Temizer, I., Wriggers, P., and Hughes, T. Contact treatment in isogeometric analysis with NURBS. *Computer Methods in Applied Mechanics and Engineering 200*, 9 (2011), 1100–1112.

[82] Temizer, I., Wriggers, P., and Hughes, T. Three-dimensional mortar-based frictional contact treatment in isogeometric analysis with nurbs. *Computer Methods in Applied Mechanics and Engineering 209* (2012), 115–128.

[83] Thomée, V. *Galerkin finite element methods for parabolic problems*, vol. 25 of *Springer Series in Computational Mathematics*. Springer-Verlag, Berlin, 1997.

[84] Wohlmuth, B. I. A mortar finite element method using dual spaces for the lagrange multiplier. *SIAM Journal on Numerical Analysis 38*, 3 (2000), 989–1012.

[85] Wriggers, P., and Zavarise, G. A formulation for frictionless contact problems using a weak form introduced by Nitsche. *Computational Mechanics 41*, 3 (2008), 407–420.

[86] Xu, G., Atroshchenko, E., and Bordas, S. Geometry-independent field approximation for spline-based finite element methods. In *Proceedings of the 11th World Congress in Computational Mechanics* (2014).

[87] Xu, G., Mourrain, B., Duvigneau, R., and Galligo, A. Parameterization of computational domain in isogeometric analysis: methods and comparison. *Computer Methods in Applied Mechanics and Engineering 200*, 23 (2011), 2021–2031.

[88] Xu, G., Mourrain, B., Duvigneau, R., and Galligo, A. Optimal analysis-aware parameterization of computational domain in 3D isogeometric analysis. *Computer-Aided Design 45*, 4 (2013), 812–821.

[89] Young, W. C., and Budynas, R. G. *Roark's formulas for stress and strain*, vol. 7. McGraw-Hill New York, 2002.

[90] Zavarise, G., Wriggers, P., and Nackenhorst, U. *A guide for engineers to computational contact mechanics*. Consorcio TCN, 2006.

[91] Zienkiewicz, O., Taylor, R., and Zhu, J. 9-The patch test, reduced integration, and non-conforming elements. In *The Finite Element Method Set (Sixth Edition)*, O. Zienkiewicz, R. Taylor, and J. Zhu, Eds., sixth edition ed. Butterworth-Heinemann, Oxford, 2005, pp. 329 – 355.